Bulletin of Earthquake Engineering
https://doi.org/10.1007/s10518-022-01338-7

ORIGINAL ARTICLE

Liquefied sites of the 2012 Emilia earthquake: a comprehensive database of the geological and geotechnical features (Quaternary alluvial Po plain, Italy)

L. Minarelli[1] · S. Amoroso[1,2] · R. Civico[3] · P. M. De Martini[3] · S. Lugli[4] · L. Martelli[5] · F. Molisso[6] · K. M. Rollins[7] · A. Salocchi[4] · M. Stefani[8] · G. Cultrera[3] · G. Milana[3] · D. Fontana[4]

Received: 6 May 2021 / Accepted: 22 January 2022

Abstract
This paper presents a comprehensive geological and geotechnical study of the whole area affected by liquefaction following the 2012 Emilia earthquakes, including all the available information from the field reconnaissance surveys, in situ tests, and laboratory analyses. The compilation was performed at 120 liquefied sites to verify and validate the reliability of liquefaction charts in alluvial sediments, and to assess liquefaction induced by the 2012 seismic sequence in the Emilia plain. The results reveal a wide range of grain sizes (from clean sands to sandy silts) and compositional characteristics (quartz-rich to litharenitic) in the 2012 ejecta, and show a strong relationship between the liquefaction and stratigraphic architecture of the subsurface. The availability of in situ tests at the liquefied sites makes it possible to verify and validate the reliability of the liquefaction charts in alluvial sediments with respect to the real observations. For the analyzed Emilia case studies, the use of non-liquefiable crust provides better estimations of the liquefaction manifestations when coupled with the thickness of the liquefiable layer rather than with the liquefaction potential index. Altogether, this work makes available to the international scientific community a consistent liquefaction database for in-depth earthquake studies.

Keywords Liquefaction database · 2012 Emilia earthquake · Field reconnaissance · Geological and geotechnical characterization · Paleochannel provenance

✉ L. Minarelli
luca.minarelli@ingv.it

1 Istituto Nazionale di Geofisica e Vulcanologia, L'Aquila, Italy

2 University of Chieti-Pescara, Pescara, Italy

3 Istituto Nazionale di Geofisica e Vulcanologia, Roma, Italy

4 University of Modena and Reggio Emilia, Modena, Italy

5 Emilia-Romagna Region, Bologna, Italy

6 Istituto di Scienze Marine CNR-ISMAR, Napoli, Italy

7 Brigham Young University, Provo, UT, USA

8 University of Ferrara, Ferrara, Italy

1 Introduction

During the last decades liquefaction case studies have been reported worldwide as a result of earthquakes with estimated magnitude $M \geq 5.4$ (Maurer et al. 2015), providing detailed information on liquefaction features and geotechnical properties (e.g. Suzuki et al. 2003; Cao et al. 2011; Green et al. 2014; Facciorusso et al. 2015; Wood et al. 2017). Data from recent earthquakes flowed into an open-source global database, the Next Generation Liquefaction project (Zimmaro et al. 2019). This project aims to improve the accessibility of coseismic effect archives and support the development of updated deterministic and probabilistic liquefaction triggering curves using the "simplified procedure", as originally introduced by Seed and Idriss (1971). These "simplified methods" for liquefaction susceptibility assessment include procedures proposed by Seed et al. (1985), Robertson and Wride (1998), Andrus and Stokoe (2000), Juang et al. (2002, 2006), Cetin et al. (2004), Moss (2003), Moss et al. (2006), Idriss and Boulanger (2008), Kayen et al. (2013), Boulanger and Idriss (2014), and Stewart et al. (2016). In this context, the 2012 Emilia (Italy) seismic sequence is of great interest because of the widespread liquefaction phenomena in Holocene alluvial sediments that have been well documented through detailed geological and geotechnical surveys (Emergeo Working Group 2013, Caputo and Papathanasiou 2012, Regione Emilia-Romagna 2012). Numerous studies have documented the liquefaction characteristics at various key sites (e.g. Amoroso et al. 2017, 2020; Lai et al. 2020; Tonni et al. 2015; Fontana et al. 2019; Meisina et al. 2019; Facciorusso et al. 2015; Civico et al. 2015; Rollins et al. 2021), but a comprehensive study of liquefaction over the whole area affected by the 2012 Emilia earthquakes, that includes both geological and geotechnical aspects, is still lacking.

The aim of the present study is to provide an unprecedented compilation of the entire set of available information, including post-earthquake surveys, in situ tests, and laboratory analyses for 120 liquefied sites. The implications of this research are twofold: (1) at a general scale, the study makes it possible to verify and validate the reliability of liquefaction triggering charts for alluvial sediments, using a significant dataset that includes a wide grain size (from clean sands to sandy silts) and compositional (quartz-rich to litharenitic) spectrum of sediments; and (2) at a regional scale, the work represents a pivotal contribution to the liquefaction assessment in the Emilia plain.

2 Geological and seismological setting

In 2012, northern Italy was hit by two mainshocks and several large aftershocks (Fig. 1; Pondrelli et al. 2012), generated by various thrust structures. The strongest shock occurred on May 20th (moment magnitude, $M_w = 6.1$), with the epicenter near the town of Finale Emilia in the Emilia-Romagna Region. Many aftershocks followed in the same area, up to the local magnitude $M_L = 5.1$. The second largest earthquake ($M_w = 5.9$) took place on May 29th to the west of the first mainshock and close to the town of Mirandola. The 2012 seismic events caused many human casualties as well as widespread damage to buildings and infrastructure (Cultrera et al. 2014).

The epicentral area of the seismic sequence, located south of the Po River (Modena, Ferrara, Bologna and Mantova provinces), was affected by the liquefaction phenomena (Fig. 1). The Emilia alluvial plain is crossed by several rivers (Fig. 1), flowing from

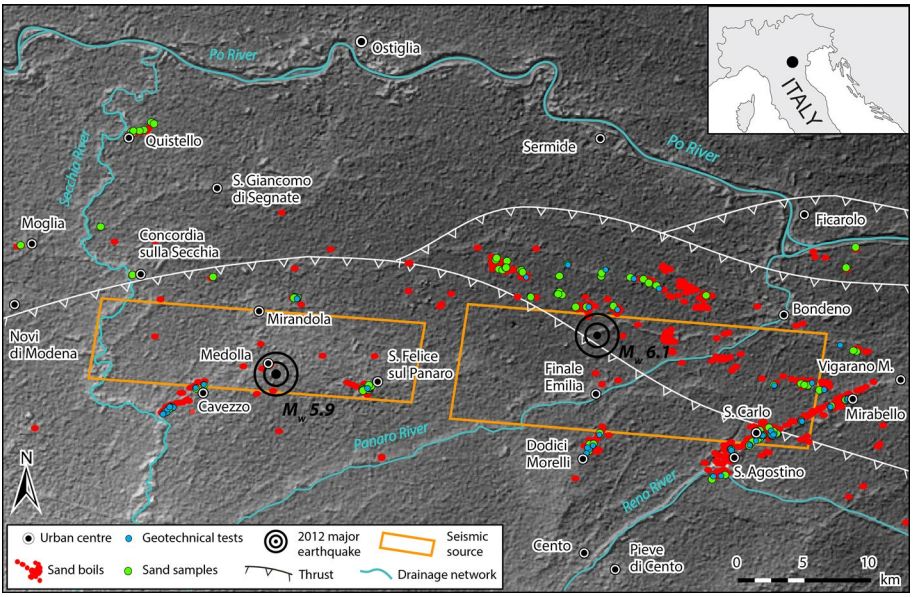

Fig. 1 Elevation model based on RADAR remote sensing image showing the geomorphological features of the study area together with the 2012 sand boils, the collected samples, the available geotechnical surveys and the fault geometries. The fault geometries are taken from the available literature and are limited to the area with source slip greater than 0 m: Pezzo et al. (2018) for the $M_W = 6.1$ on May 20th and Paolucci et al. (2015) for the $M_W = 5.9$ on May 29th

the Apennines into the Po River (Secchia, Panaro), or directly reaching the Adriatic Sea (Reno). The alluvial plain is the surface expression of the foredeep basin of the Apennine chain, where the combination of fast subsidence and strong sediment input generated very thick Plio-Pleistocene successions (Ghielmi et al. 2010). The study area corresponds to the buried frontal portion of the compressive ramp and flat structures of the Apennines (Toscani et al. 2009; Martelli et al. 2017). The active faults are associated with moderate seismic activity (Michetti et al. 2012), characterized by shallow epicenters, well documented through the last centuries (Locati et al. 2011; Guidoboni et al. 2018). However, taking into account the social and economic regional context, the related expected seismic risk is rather high. The most significant historic earthquake, that impacted the Ferrara area in November 1570 (VIII MCS, estimated moment magnitude $M_w = 5.5$), induced sand liquefaction and ground fracturing, both within the town of Ferrara (Guidoboni et al. 2018) and in the Reno River sediments at San Carlo, that also exhibited liquefaction in 2012 (Caputo et al. 2016).

Both the 2012 mainshocks triggered widespread liquefaction of granular sediments, sand boils, ground fractures, and gravitational lateral spreading. The liquefaction phenomena in the eastern sector of San Felice sul Panaro were mainly associated with the mainshock of the 2012 May 20th, whereas those in the western sector were coupled with the May 29th earthquake. It is worthy of note that at some sites liquefaction phenomena (e.g. San Felice sul Panaro) have been observed following both the May 20th and 29th shocks (Pizzi and Scisciani 2012; Emergeo Working Group 2013). Moreover, the May 20th aftershocks, occurred within a close time interval (less than 4 minutes with M_L between 4.8 and

5.0), may have had some effects on pore water pressure build-up within the saturated cohesionless layers, especially in the municipality of Terre del Reno (villages of Sant'Agostino, San Carlo, Mirabello) where the most and largest liquefaction effects were observed (Sinatra and Foti 2015; Facciorusso et al. 2016).

Liquefaction mainly took place within fluvial channel deposits. A strong relationship exists between the siting of the liquefaction and the stratigraphic architecture of the subsurface. The liquefaction sites are typically confined to elongated strips, corresponding to fluvial buried sandy bodies of Holocene age (Civico et al. 2015). The sites analyzed in the present research consider the geotechnical investigations available approximately in the upper 30 m of depth, where the stratigraphic interval consists of late Pleistocene and Holocene deposits. The interval is divided into two superposed subsynthems: the upper Pleistocene AES7 and the Holocene AES8 (Stefani et al. 2018). The ejected liquefied sands sampled at the surface derive entirely from the Holocene units, in particular from sediments younger than roughly 4000 years.

The analyzed deposits record two main sediment inputs, fed by the Po River to the north, and by several streams flowing from the Apennine chain to the south (Secchia, Panaro and Reno rivers; Fig. 1). The Po River largely differs from the Apennines counterparts in its fluvial dynamics, grain size distribution, and petrographic composition. The two fluvial systems therefore generated sharply different sediments, in the northern and southern portions of the research areas, respectively.

During synglacial times (AES7 unit), the Po deposited large coarse sand bodies into braided river environments, whereas during the Holocene (AES8), it sedimented finer grained sands into meandering channels. The Holocene meander channels often reworked the upper Pleistocene deposits, generating thick continuous bodies of sands. The depositional geometry and geomorphic expression of some of the younger meander bodies are visible at the surface (Figs. 2b and c). During the last millennia, the Po started to generate hanging channels, less curved in plan, interspaced with interfluvial depressions, where finer grained sediments accumulated.

The Apennine rivers also provided large volumes of sediments, but finer grained compared to the Po deposits. During the last glaciation, great volumes of silt and argillaceous silt accumulated, framing thin bodies of fluvial sands (AES7). During the Holocene, the rivers flowing from the Apennine valleys produced large volumes of clayey or silty

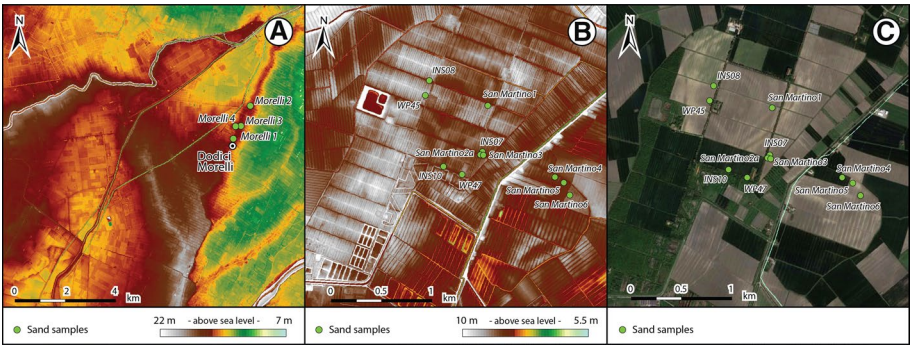

Fig. 2 LIDAR and satellite images: (**a**) fluvial ridges of the inner delta of the medieval Reno River (Cento), (**b**) pre-Roman meanders of the Po River (San Martino in Spino) and (**c**) a satellite image of the same area illustrated in (b). Green dots depict coseismic liquefaction sand boils

sediments, often rich in peat and formed flood plains and freshwater marshes, framing isolated fluvial channel bodies, mainly consisting of silty sands. Throughout the last millennia, the boundary between the deposits of the Apennine rivers and of the Po River progressively migrated northward. In medieval times, the Apennine rivers were unable to flow into the Po and formed large inland delta systems (Fig. 2a). The inland distributary channels of the Secchia, Panaro and Reno rivers prograded into large freshwater marshes and shallow lakes. A significant portion of the liquefied sands analyzed in the southern part of the study region accumulated in these inland delta distributary channels, which often maintain a strong topographic expression, as elongated ridges (Fig. 2a).

3 Methods

3.1 Field survey and sampling

The detailed 2012 field reconnaissance survey identified different coseismic geological features associated with liquefaction or fracture/liquefaction. These features include single sand volcanoes, scattered vents, coalescent flat cones, sand infilled water wells, fountains and manholes, elongated and aligned multiple sand volcanoes and sand flows from open fractures. Examples of these liquefaction features are reported in the photos in Fig. 3.

A total of 120 sites were analyzed and sampled in the alluvial plain area located between the Po, Reno and Secchia rivers in the Ferrara, Modena, Bologna and Mantova provinces

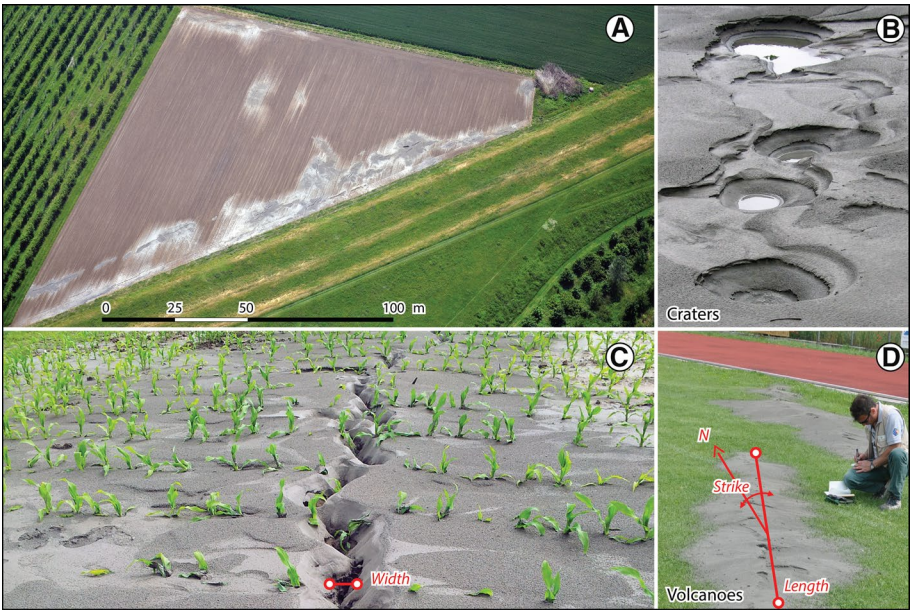

Fig. 3 Field survey photos of liquefaction evidences: (**a**) aerial image of extended sand ejecta (Pieve di Cento), (**b**) multiple craters (San Carlo), (**c**) sand ejected along a fracture (San Carlo), and (**d**) aligned volcanoes (San Felice sul Panaro). More images (Emergeo Working Group 2012) are available at https://istituto.ingv.it/images/collane-editoriali/miscellanea/miscellanea-2012/miscellanea16.pdf

(Fig. 1). For the liquefaction sites we report, when available, structural and morphological data including: (1) morphology, diameter and thickness of the sand boils; (2) spacing, including length and strike of the sand boil alignments and associated fractures. The thickness of the extruded sand was up to about 40 cm, the maximum observed diameter of individual sand volcanoes was 10 m, and the coalescent sand volcanoes along fractures extended for a maximum length of 50 m (Emergeo Working Group 2013). Samples of the liquefied extruded sand were collected for sedimentological analysis. The samples were preserved in plastic bags and their weight was commonly between 200 and 500 grams. Moreover, qualitative surveys of liquefaction-induced land damage related to 2012 Emilia earthquakes were performed by means of a reappraisal of field and aerial identification and characterization of liquefaction phenomena. The land damage estimation was carried out following the qualitative scale proposed by van Ballegooy et al. (2014):

- *Category 1* - No observed ground cracking or ejected liquefied material;
- *Category 2* - Minor ground cracking but not observed ejected liquefied material;
- *Category 3* - No lateral spreading but minor to moderate quantities of ejected material;
- *Category 4* - No lateral spreading but large quantities of ejected material;
- *Category 5* - Moderate to major lateral spreading; ejected material often observed;
- *Category 6* - Severe lateral spreading; ejected material often observed.

This estimation is clearly relative to the 2012 damage and Categories 1 and 2 were not considered since the 120 analyzed sites are all liquefied sites with ejected material. For each site a detailed report sheet has been compiled (see electronic supplement of this paper).

3.2 Grain size and compositional analyses

A total of 120 sand boil samples were analyzed using standard techniques. To reduce sampling bias due to possible segregation of particle sizes during the sand boil formation, for each site we sampled the complete vertical sequence next to the ejection point; the deposit normally did not exceed 10 cm in thickness. For comparison, two additional samples (San Martino 2b and San Martino 6bis; see the electronic supplement of this paper) were also collected from the fine-grained distal portion of the ejected deposits. These samples are not plotted in the graph of the Figs. 4 and 5, presented in the next sections of the work, as they are not representative of the complete ejected deposit.

Mechanical sieving was performed for the sandy fraction along with hydrometer analysis or laser diffractometry analysis for the fine-grained sediments. Sand samples consisting of a few hundred grams were washed with dilute H_2O_2 to remove organic matter and were air dried and mechanically sieved for grain size and compositional analyses.

Compositional analyses were carried out on sand samples by point counting (300 grains for each thin section) under transmitted-light microscopy. Analyses were performed on the 0.125–0.250 mm fraction, according to the Gazzi-Dickinson method designed to minimize the dependence of the analysis on the grain size (Zuffa 1985) and to support a comparison with previous compositional studies performed in the area (Lugli et al. 2004, 2007). The aim of the compositional study was to attribute the ejected sand to the specific buried fluvial channels of the alluvial system (Po, Secchia, Panaro and Reno rivers). Sorting was calculated according to Folk and Ward (1957) using the GRADISTAT software.

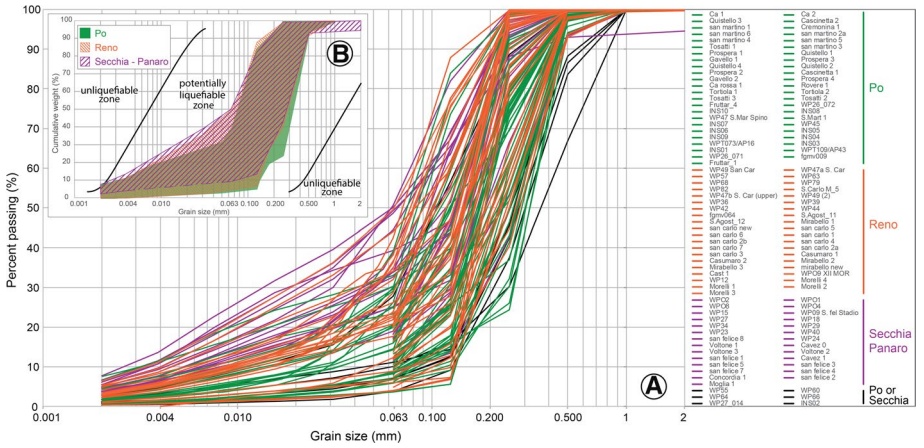

Fig. 4 (**a**) Cumulative grain size curves of examined sand blows. The colors refer to sand blow location and paleochannel attribution. (**b**) Cumulative curve envelopes for the main paleochannels compared with the liquefiable zone limits defined by Tsuchida and Hayashi (1971)

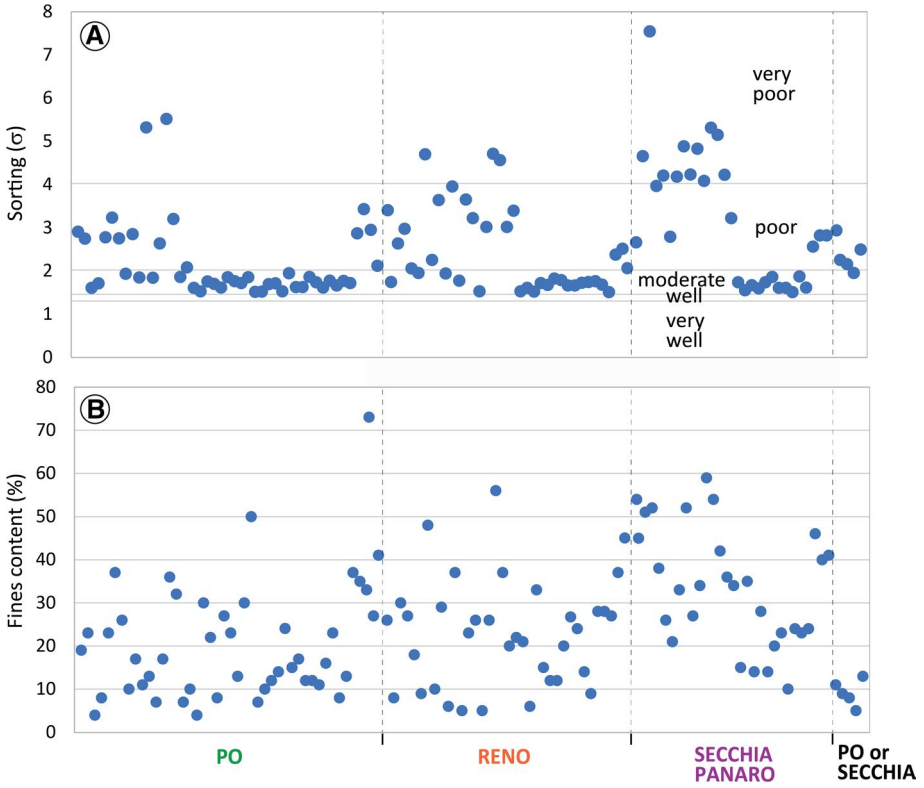

Fig. 5 Plot showing the sorting (**a**) and fine content (**b**) of all sand blows according to the paleochannel attribution. Most samples are moderate to poorly sorted

3.3 Geotechnical investigation

The presented work benefitted greatly from the large dataset of previous geological-geotechnical subsurface investigations, developed by the Emilia-Romagna Regional Administration (https://ambiente.regione.emilia-romagna.it/it/geologia/cartografia/webgis-banchedati/banca-dati-geognostica). The available dataset, compiled since the early 1990s, provides more than 65,000 logs, throughout the alluvial plain, including more than 5,000 piezocone penetration tests (about 1,000 are located within the epicentral region of the 2012 earthquake), deriving from microzonation studies and reconstruction projects developed after the seismic crisis (Regione Emilia-Romagna 2013; Martelli et al. 2013). The dataset of the 120 sites includes the available piezocone tests (CPTU), electrical cone penetration tests (CPTE), dilatometer tests (DMT), seismic dilatometer tests (SDMT) and boreholes with standard penetration tests (SPT) performed at the liquefied sites or in their proximity.

4 Data analysis

Relevant data for all 120 liquefaction sites has been assembled and analyzed. For each site, a comprehensive dataset has been developed including geographical and morphological data, liquefaction features, liquefaction-induced land damage and related seismic parameters. In addition, grain size and compositional analyses, paleoriver assignment, and geotechnical tests were assembled. Finally, liquefaction assessments have been performed using in situ tests. These data are organized as a single report sheet presented in the electronic supplement of this paper and are summarized in Table 1.

4.1 Sand boil characterization: grain-size, texture and composition

4.1.1 Grain size analysis

Sand blows show variable grain size distributions as illustrated in the cumulative curves of Fig. 4 and in Table 1. The index properties for each sand blow were estimated using the grain size distribution, and include (Table 1):

- the fines content (FC) which represents the percentage of particles finer than 0.075 mm;
- the coefficient of uniformity (U), given by the equation:

$$U = \frac{D_{60}}{D_{10}} \tag{1}$$

  where D_x is the diameter of the generic xth percentile of the grain size curve;
- the coefficient of curvature (C), given by the equation:

$$C = \frac{(D_{30})^2}{D_{10} \cdot D_{60}} \tag{2}$$

- the sorting (σ), given by the equation:

Table 1 Summary information of the 120 analyzed test sites

Test site	Municipality	Location	Morphology	Paleochannel	FC (%)	U	C	σ	USCS classification	Land damage category	CPT test
Ca 1	Bondeno	Salvatonica	Flat interfluvial depression	Po		21.33	3.31	2.88	Silty Sand (SM)	3	No
Casc1	Bondeno	Cascinetta	Flat interfluvial depression	Po	13	2.92	1.37	–	Silty Sand (SM)	3	No
Casc2	Bondeno	Cascinetta	Flat interfluvial depression	Po	37	3.42	1.46	–	Silty Sand (SM)	4	No
Cremonina 1	Bondeno	Cascinetta	Flat interfluvial depression	Po	14	–	–	1.72	Silty Sand (SM)	4	No
fgmv009	Bondeno	Bondeno	Flat interfluvial depression	Po	37	13.68	3.42	0.08	Silty Sand (SM)	4	No
Fruttar_4	Bondeno	Cascinetta	Flat interfluvial depression	Po	10	2.93	1.55	1.94	Poorly graded sand with silt (SP–SM)	4	No
Gavello 1	Bondeno	Redena	Fluvial ridge	Po	8	3.82	1.31	1.70	Poorly graded sand with silt (SP–SM)	3	Yes
Gavello 2	Bondeno	Gavello	Flat interfluvial depression	Po	27	–	–	1.62	Silty Sand (SM)	3	Yes
INS04	Bondeno	Redena	Fluvial ridge	Po	7	2.62	1.20	1.84	Poorly graded sand with silt (SP–SM)	3	Yes
INS05	Bondeno	Redena	Flat interfluvial depression	Po	17	6.67	2.40	2.64	Silty Sand (SM)	3	No
INS06	Bondeno	Gavello	Flat interfluvial depression	Po	36	53.13	2.94	5.52	Silty Sand (SM)	3	Yes
INS09	Bondeno	Redena	Fluvial ridge	Po	10	4.00	1.28	2.09	Poorly graded sand with silt (SP–SM)	3	Yes

Table 1 (continued)

Test site	Municipality	Location	Morphology	Paleochannel	FC (%)	U	C	σ	USCS classification	Land damage category	CPT test
Prospera1	Bondeno	Gavello	Fluvial ridge	Po	23	–	–	1.86	Silty Sand (SM)	4	Yes
Prospera2	Bondeno	Gavello	Fluvial ridge	Po	13	3.91	1.41	1.77	Silty Sand (SM)	4	No
Prospera3	Bondeno	Gavello	Fluvial ridge	Po	30	–	–	1.71	Silty Sand (SM)	4	Yes
Rovere1	Bondeno	Gavello	Flat interfluvial depression	Po	13	–	–	1.78	Silty Sand (SM)	4	No
San Martino4	Bondeno	Redena	Flat interfluvial depression	Po	17	–	–	1.63	Silty Sand (SM)	4	No
San Martino5	Bondeno	Redena	Flat interfluvial depression	Po	12	3.08	1.51	1.63	Poorly graded sand with silt (SP–SM)	4	No
San Martino6	Bondeno	Redena	Flat interfluvial depression	Po	12	3.86	1.04	1.86	Poorly graded sand with silt (SP–SM)	4	No
San Martino6bis	Bondeno	Redena	Flat interfluvial depression	Po	41	4.52	1.99	2.12	Silty Sand (SM)	4	No
Tosatti 1	Bondeno	Gavello	Flat interfluvial depression	Po	30	–	–	1.54	Silty Sand (SM)	4	No
Tosatti 2	Bondeno	Gavello	Flat interfluvial depression	Po	22	–	–	1.76	Silty Sand (SM)	3	No
WP26_071	Bondeno	Scortichino	Flat interfluvial depression	Po	4	1.79	0.93	1.61	Poorly graded sand (SP)	4	No
WP26_072	Bondeno	Cascinetta	Flat interfluvial depression	Po	8	2.60	1.75	1.72	Poorly graded sand with silt (SP–SM)	4	No
WP39	Bondeno	Casumaro	Flat interfluvial depression	Reno	30	8.06	2.53	2.63	Silty Sand (SM)	4	Yes

Table 1 (continued)

Test site	Municipality	Location	Morphology	Paleochannel	FC (%)	U	C	σ	USCS classification	Land damage category	CPT test
WP42	Bondeno	Casumaro	Flat interfluvial depression	Reno	27	17.35	3.84	2.98	Silty Sand (SM)	4	Yes
WP44	Bondeno	Casumaro	Flat interfluvial depression	Reno	18	3.62	1.80	2.07	Silty Sand (SM)	4	Yes
Cavez 0	Cavezzo	Cavezzo	Fluvial ridge	Secchia	46	12.5	2.53	2.57	Silty Sand (SM)	4	Yes
Cavez 1	Cavezzo	Cavezzo	Fluvial ridge	Secchia	15	–	–	1.74	Silty Sand (SM)	4	Yes
Voltone1	Cavezzo	Cavezzo	Fluvial ridge	Secchia	41	20.00	3.47	2.83	Silty Sand (SM)	4	Yes
Voltone2	Cavezzo	Cavezzo	Fluvial ridge	Secchia	10	4.13	1.47	1.61	Poorly graded sand with silt (SP–SM)	4	Yes
Voltone3	Cavezzo	Cavezzo	Fluvial ridge	Secchia	24	–	–	1.52	Silty Sand (SM)	3	Yes
WP23	Cavezzo	Voltone	Fluvial ridge	Secchia	54	35.19	0.76	5.32	Sandy Silt (ML)	4	Yes
WP24	Cavezzo	Voltone	Fluvial ridge	Secchia	42	41.03	0.52	5.15	Silty Sand (SM)	4	Yes
Morelli1	Cento	Dodici Morelli	Fluvial ridge	Reno	37	8.67	2.17	2.38	Silty Sand (SM)	3	Yes
Morelli2	Cento	Dodici Morelli	Fluvial ridge	Reno	28	–	–	1.69	Silty Sand (SM)	3	Yes
Morelli3	Cento	Dodici Morelli	Fluvial ridge	Reno	27	–	–	1.51	Sandy Silt (ML)	4	Yes
Morelli4	Cento	Dodici Morelli	Fluvial ridge	Reno	45	9.50	2.63	2.52	Silty Sand (SM)	4	Yes
WP09 XII Mor	Cento	Dodici Morelli	Fluvial ridge	Reno	26	20.59	6.46	3.41	Silty Sand (SM)	4	Yes
WP12	Cento	Dodici Morelli	Fluvial ridge	Reno	26	20.63	6.14	3.23	Silty Sand (SM)	4	Yes
Concordia 1	Concordia sul Secchia	Concordia sul Secchia	Fluvial ridge	Secchia	23	–	–	1.88	Silty Sand (SM)	3	No
WP27_014	Concordia sul Secchia	Concordia sul Secchia	Flat interfluvial depression	Secchia	34	10.77	2.54	3.22	Silty Sand (SM)	3	No
Ca 2	Ferrara	Porporana	Fluvial ridge	Po	33	66.67	6.62	3.44	Silty Sand (SM)	3	No

Table 1 (continued)

Test site	Municipality	Location	Morphology	Paleochannel	FC (%)	U	C	σ	USCS classification	Land damage category	CPT test
ca rossa 1	Finale Emilia	Rossa	Flat interfluvial depression	Po	8	4.24	2.21	1.67	Poorly graded sand with silt (SP–SM)	4	No
Fruttar_1	Finale Emilia	Finale Emilia	Flat interfluvial depression	Po	26	12.31	3.39	2.76	Silty Sand (SM)	3	No
INS07	Mirandola	San Martino Spino	Flat interfluvial depression	Po	32	12.80	2.54	3.21	Silty Sand (SM)	4	No
INS08	Mirandola	San Martino Spino	Flat interfluvial depression	Po	7	2.58	1.02	1.87	Poorly graded sand with silt (SP–SM)	4	No
INS10	Mirandola	San Martino Spino	Flat interfluvial depression	Po	4	2.00	0.83	1.61	Poorly graded sand (SP)	3	No
S.Mart1	Mirandola	San Martino Spino	Flat interfluvial depression	Po	17	0.83	0.26	2.86	Silty Sand (SM)	4	No
San Martino1	Mirandola	San Martino Spino	Flat interfluvial depression	Po	24	–	–	1.53	Silty Sand (SM)	4	No
San Martino 2a	Mirandola	San Martino Spino	Flat interfluvial depression	Po	27	–	–	1.95	Silty Sand (SM)	4	No
San Martino 2b	Mirandola	San Martino Spino	Flat interfluvial depression	Po	73	13.89	2.45	2.95	Silt with sand (ML)	4	No
San Martino3	Mirandola	San Martino Spino	Flat interfluvial depression	Po	15	–	–	–	Silty Sand (SM)	4	No
WP45	Mirandola	San Martino Spino	Flat interfluvial depression	Po	19	7.14	2.57	2.91	Silty Sand (SM)	4	No
WP47 San Mar Spino	Mirandola	San Martino Spino	Flat interfluvial depression	Po	9	3.13	1.19	1.96	Poorly graded sand with silt (SP–SM)	3	No

Table 1 (continued)

Test site	Municipality	Location	Morphology	Paleochannel	FC (%)	U	C	σ	USCS classification	Land damage category	CPT test
WP55	Mirandola	Cividale	Flat interfluvial depression	Secchia or Po	11	5.38	2.75	2.94	Poorly graded sand with silt (SP–SM)	4	Yes
WP60	Mirandola	Cividale	Flat interfluvial depression	Secchia or Po	9	3.67	1.22	2.26	Poorly graded sand with silt (SP–SM)	4	Yes
WP64	Mirandola	Cividale	Flat interfluvial depression	Secchia or Po	8	3.16	1.01	2.16	Poorly graded sand with silt (SP–SM)	4	Yes
WP66	Mirandola	Cividale	Flat interfluvial depression	Secchia or Po	5	2.77	0.94	1.96	Poorly graded sand with silt (SP–SM)	4	Yes
Moglia1	Moglia	Moglia	Flat interfluvial depression	Secchia	24	17.35	3.84	1.62	Silty Sand (SM)	4	No
Reno1	Pieve di Cento	La Bisana	Flat interfluvial depression	Reno	24	–	–	–	Silty Sand (SM)	3	Yes
Reno2	Pieve di Cento	La Bisana	Flat interfluvial depression	Reno	7	2.67	1.15	–	Poorly graded sand with silt (SP–SM)	4	Yes
INS01	Quistello	Quistello	Flat interfluvial depression	Po	11	2.86	1.61	1.85	Poorly graded sand with silt (SP–SM)	4	No
Quist1	Quistello	Quistello	Flat interfluvial depression	Po	7	3.30	1.89	1.52	Poorly graded sand with silt (SP–SM)	4	No

Table 1 (continued)

Test site	Municipality	Location	Morphology	Paleochannel	FC (%)	U	C	σ	USCS classification	Land damage category	CPT test
Quist2	Quistello	Quistello	Flat interfluvial depression	Po	10	4.80	2.50	1.53	Poorly graded sand with silt (SP–SM)	3	No
Quist3	Quistello	Quistello	Flat interfluvial depression	Po	50	3.87	1.13	–	Sandy Silt (ML)	3	No
Quist4	Quistello	Quistello	Flat interfluvial depression	Po	12	4.21	1.32	1.70	Silty Sand (SM)	3	No
WPT073/AP16	Quistello	Quistello	Flat interfluvial depression	Po	23	12.00	3.70	2.78	Silty Sand (SM)	4	No
WPT109/AP43	Quistello	Quistello	Flat interfluvial depression	Po	23	6.80	2.12	2.75	Silty Sand (SM)	4	No
San Felice1	San Felice sul Panaro	San Felice sul Panaro	Fluvial ridge	Panaro – Secchia	35	–	–	1.55	Silty Sand (SM)	4	No
San Felice2	San Felice sul Panaro	San Felice sul Panaro	Fluvial ridge	Panaro – Secchia	14	–	–	1.67	Silty Sand (SM)	4	No
San Felice3	San Felice sul Panaro	San Felice sul Panaro	Fluvial ridge	Panaro – Secchia	28	–	–	1.60	Silty Sand (SM)	4	No
San Felice4	San Felice sul Panaro	San Felice sul Panaro	Fluvial ridge	Panaro – Secchia	14	–	–	1.74	Silty Sand (SM)	3	No
San Felice5	San Felice sul Panaro	San Felice sul Panaro	Fluvial ridge	Panaro – Secchia	20	–	–	1.87	Silty Sand (SM)	3	No
San Felice7	San Felice sul Panaro	San Felice sul Panaro	Fluvial ridge	Panaro – Secchia	23	–	–	1.61	Silty Sand (SM)	3	No
San Felice8	San Felice sul Panaro	San Felice sul Panaro	Fluvial ridge	Panaro – Secchia	40	15.56	1.98	2.82	Silty Sand (SM)	3	No

Table 1 (continued)

Test site	Municipality	Location	Morphology	Paleochannel	FC (%)	U	C	σ	USCS classification	Land damage category	CPT test
WP01	San Felice sul Panaro	San Felice sul Panaro	Fluvial ridge	Panaro – Secchia	51	25.00	1.69	4.66	Sandy Silt (ML)	3	No
WP02	San Felice sul Panaro	San Felice sul Panaro	Fluvial ridge	Panaro – Secchia	52	31.25	1.13	7.55	Sandy Silt (ML)	3	No
WP04	San Felice sul Panaro	San Felice sul Panaro	Fluvial ridge	Panaro – Secchia	38	25.00	3.87	3.97	Silty Sand (SM)	4	No
WP08	San Felice sul Panaro	San Felice sul Panaro	Fluvial ridge	Panaro – Secchia	26	30.00	11.20	4.21	Silty Sand (SM)	4	No
WP09 San fel Stadio	San Felice sul Panaro	San Felice sul Panaro	Fluvial ridge	Panaro – Secchia	36	29.09	2.84	4.23	Silty Sand (SM)	4	No
WP15	San Felice sul Panaro	San Felice sul Panaro	Fluvial ridge	Panaro – Secchia	21	10.59	5.52	2.80	Silty Sand (SM)	4	No
WP18	San Felice sul Panaro	San Felice sul Panaro	Fluvial ridge	Panaro – Secchia	33	29.10	4.51	4.19	Silty Sand (SM)	4	No
WP27	San Felice sul Panaro	San Felice sul Panaro	Fluvial ridge	Panaro – Secchia	52	31.43	1.15	4.89	Sandy Silt (ML)	4	No
WP29	San Felice sul Panaro	San Felice sul Panaro	Fluvial ridge	Panaro – Secchia	27	29.23	7.31	4.24	Silty Sand (SM)	4	No
WP34	San Felice sul Panaro	San Felice sul Panaro	Fluvial ridge	Panaro – Secchia	34	35.56	2.81	4.83	Silty Sand (SM)	4	No
WP40	San Felice sul Panaro	San Felice sul Panaro	Fluvial ridge	Panaro – Secchia	59	17.78	1.47	4.09	Sandy Silt (ML)	4	No
INS02	San Giacomo delle Segnate	Stoffi	Flat interfluvial depression	Secchia or Po	13	6.67	2.40	2.50	Silty Sand (SM)	3	No
Cast1	Terre del Reno	Mirabello	Flat interfluvial depression	Reno	21	–	–	1.53	Silty Sand (SM)	4	Yes

Table 1 (continued)

Test site	Municipality	Location	Morphology	Paleochannel	FC (%)	U	C	σ	USCS classification	Land damage category	CPT test
Casum1	Terre del Reno	Casumaro	Flat interfluvial depression	Reno	6	2.30	1.26	1.61	Poorly graded sand with silt (SP–SM)	4	Yes
Casum2	Terre del Reno	Casumaro	Flat interfluvial depression	Reno	33	–	–	1.53	Silty Sand (SM)	4	Yes
fgmv064	Terre del Reno	Casumaro	Flat interfluvial depression	Reno	5	1.53	0.98	1.53	Poorly graded sand with silt (SP–SM)	4	Yes
Mirabello new	Terre del Reno	Mirabello	Fluvial ridge	Reno	12	4.61	1.48	1.83	Silty Sand (SM)	5	Yes
Mirabello1	Terre del Reno	Mirabello	Fluvial ridge	Reno	48	19.00	2.88	–	Silty Sand (SM)	6	Yes
Mirabello2	Terre del Reno	Mirabello	Fluvial ridge	Reno	15	–	–	1.72	Silty Sand (SM)	4	Yes
Mirabello3	Terre del Reno	Mirabello	Fluvial ridge	Reno	12	–	–	1.68	Silty Sand (SM)	5	Yes
WP36	Terre del Reno	Casumaro	Flat interfluvial depression	Reno	8	1.33	0.56	1.75	Poorly graded sand with silt (SP–SM)	4	Yes
WP47 San Car (upper)	Terre del Reno	Casumaro	Flat interfluvial depression	Reno	22	18.95	9.88	3.40	Silty Sand (SM)	3	Yes
WP47a San Car	Terre del Reno	Casumaro	Flat interfluvial depression	Reno	10	3.26	1.26	2.26	Poorly graded sand with silt (SP–SM)	3	Yes
S.Agost_11	Terre del Reno	Sant'Agostino	Fluvial ridge	Reno	26	16.82	0.04	3.02	Silty Sand (SM)	4	Yes
S.Agost_12	Terre del Reno	Sant'Agostino	Fluvial ridge	Reno	56	22.86	1.29	4.71	Sandy Silt (ML)	4	Yes
San Carlo M_5	Terre del Reno	San Carlo	Fluvial ridge	Reno	37	35.60	2.22	4.57	Silty Sand (SM)	6	No
San Carlo new	Terre del Reno	San Carlo	Fluvial ridge	Reno	43	13.33	1.88	–	Silty Sand (SM)	6	Yes
San Carlo1	Terre del Reno	San Carlo	Fluvial ridge	Reno	20	–	–	1.79	Silty Sand (SM)	5	Yes
San Carlo2b	Terre del Reno	San Carlo	Fluvial ridge	Reno	24	–	–	1.67	Silty Sand (SM)	5	Yes

Table 1 (continued)

Test site	Municipality	Location	Morphology	Paleochannel	FC (%)	U	C	σ	USCS classification	Land damage category	CPT test
San Carlo3	Terre del Reno	San Carlo	Fluvial ridge	Reno	14	2.07	0.80	1.78	Silty Sand (SM)	5	Yes
San Carlo4	Terre del Reno	San Carlo	Fluvial ridge	Reno	9	4.00	1.41	1.75	Poorly graded sand with silt (SP–SM)	5	Yes
San Carlo5	Terre del Reno	San Carlo	Flat interfluvial depression	Reno	54	5.33	1.33	2.07	Sandy Silt (ML)	5	No
San Carlo6	Terre del Reno	San Carlo	Flat interfluvial depression	Reno	45	10.56	2.92	2.67	Silty Sand (SM)	5	No
San Carlo7	Terre del Reno	San Carlo	Flat interfluvial depression	Reno	28	–	–	1.77	Silty Sand (SM)	3	Yes
Tosatti 3	Terre del Reno	San Carlo	Flat interfluvial depression	Po	23	–	–	1.78	Silty Sand (SM)	3	No
WP49 san car	Terre del Reno	San Carlo	Flat interfluvial depression	Reno	48	32.50	1.20	4.70	Silty Sand (SM)	4	Yes
WP49(2)	Terre del Reno	San Carlo	Flat interfluvial depression	Reno	20	15.83	8.60	3.02	Silty Sand (SM)	4	Yes
WP57	Terre del Reno	San Carlo	Fluvial ridge	Reno	29	22.67	4.89	3.64	Silty Sand (SM)	6	Yes
WP63	Terre del Reno	San Carlo	Flat interfluvial depression	Reno	6	2.30	0.93	1.94	Poorly graded sand with silt (SP–SM)	4	Yes
WP68	Terre del Reno	San Carlo	Flat interfluvial depression	Reno	37	21.67	3.88	3.96	Silty Sand (SM)	4	No
WP79	Terre del Reno	San Carlo	Fluvial ridge	Reno	5	2.07	0.80	1.78	Poorly graded sand with silt (SP–SM)	5	Yes
WP82	Terre del Reno	San Carlo	Fluvial ridge	Reno	23	20.52	9.12	3.66	Silty Sand (SM)	5	Yes

Table 1 (continued)

Test site	Municipality	Location	Morphology	Paleochannel	FC (%)	U	C	σ	USCS classification	Land damage category	CPT test
Tortiola1	Vigarano Mainarda	Tortiola	Fluvial ridge	Po	11	–	–	1.62	Silty Sand (SM)	4	Yes
Tortiola2	Vigarano Mainarda	Tortiola	Fluvial ridge	Po	16	4.29	1.38	1.74	Poorly graded sand with silt (SP–SM)	4	Yes

Test site	Depth of in situ GWT (m)	Depth of earthquake GWT (m)	a_{max}	M_w	LPI	LSN	S(m)	Depth of liquefiable layer (m)	H_2 (m)	H_1 (m)	$CSR_{7.5avg}$	$I_{c\ avg}$	$q_{C1N\ avg}$
Ca 1	–	–	–	–	–	–	–	–	–	–	–	–	–
Casc1	–	–	–	–	–	–	–	–	–	–	–	–	–
Casc2	–	–	–	–	–	–	–	–	–	–	–	–	–
Cremonina 1	–	–	–	–	–	–	–	–	–	–	–	–	–
fgmv009	–	–	–	–	–	–	–	–	–	–	–	–	–
Fruttar_4	–	–	–	–	–	–	–	–	–	–	–	–	–
Gavello 1	3	3	0.40	6.10	*20.96*	**27.78**	*0.29*	4.3–8.7	4.4	4.3	0.23	2.15	44.14
Gavello 2	3	1	0.42	6.10	*17.01*	**18.84**	*0.24*	5.6–12.2	6.6	5.6	0.31	2.26	50.71
INS04	3	3	0.40	6.10	*20.96*	**27.78**	*0.29*	4.3–8.7	4.4	4.3	0.23	2.15	44.14
INS05	–	–	–	–	–	–	–	–	–	–	–	–	–
INS06	3	1	0.41	6.10	*18.55*	**21.31**	**0.16**	4.2–9.3	5.1	4.2	0.30	2.26	46.05
INS09	3	3	0.40	6.10	*20.96*	**27.78**	*0.29*	4.3–8.7	4.4	4.3	0.23	2.15	44.14
Prospera1	3	3	0.42	6.10	**13.73**	**18.13**	**0.23**	5.6–12.2	6.6	5.6	0.25	2.26	49.94

Table 1 (continued)

Test site	Depth of in situ GWT (m)	Depth of earthquake GWT (m)	a_{max}	M_w	LPI	LSN	S(m)	Depth of liquefiable layer (m)	H_2 (m)	H_1 (m)	$CSR_{7.5avg}$	$I_{c\ avg}$	$q_{C1N\ avg}$
Prospera2	–	–	–	–	–	–	–	–	–	–	–	–	–
Prospera3	3	3	0.43	6.10	**7.43**	***9.35***	**0.13**	10.0–15.9	5.9	10.0	0.26	2.25	50.97
Rovere1	–	–	–	–	–	–	–	–	–	–	–	–	–
San Martino4	–	–	–	–	–	–	–	–	–	–	–	–	–
San Martino5	–	–	–	–	–	–	–	–	–	–	–	–	–
San Martino6	–	–	–	–	–	–	–	–	–	–	–	–	–
San Martino-6bis	–	–	–	–	–	–	–	–	–	–	–	–	–
Tosatti 1	–	–	–	–	–	–	–	–	–	–	–	–	–
Tosatti 2	–	–	–	–	–	–	–	–	–	–	–	–	–
WP26_071	–	–	–	–	–	–	–	–	–	–	–	–	–
WP26_072	–	–	–	–	–	–	–	–	–	–	–	–	–
WP39	3	1	0.46	6.10	**24.27**	***26.66***	**0.40**	5.8–20.0	14.2	5.8	0.31	1.85	83.42
WP42	3	1	0.46	6.10	**24.27**	***26.66***	**0.40**	5.8–20.0	14.2	5.8	0.31	1.85	83.42
WP44	3	1	0.46	6.10	**24.27**	***26.66***	**0.40**	5.8–20.0	14.2	5.8	0.31	1.85	83.42
Cavez 0	3	3	0.42	5.90	***4.16***	***5.92***	***0.04***	7.4–8.2	0.8	7.4	0.23	2.28	37.67
Cavez 1	3	3	0.42	5.90	***0.85***	***1.76***	***0.01***	3.8–4.2	0.6	3.8	0.19	2.60	22.64
Voltone1	3	3	0.40	5.90	**17.99**	***28.12***	**0.16**	3.5–8.7	5.2	3.5	0.21	1.91	47.89
Voltone2	3	3	0.40	5.90	**16.86**	***28.60***	**0.16**	3.0–8.6	5.6	3.0	0.20	1.95	50.88
Voltone3	3	3	0.39	5.90	**6.75**	***14.30***	**0.10**	3.0–5.2	2.2	3.0	0.18	2.42	46.00
WP23	3	3	0.40	5.90	**17.99**	***28.12***	**0.16**	3.5–8.7	5.2	3.5	0.21	1.91	47.89

Table 1 (continued)

Test site	Depth of in situ GWT (m)	Depth of earthquake GWT (m)	a_{max}	M_w	LPI	LSN	S(m)	Depth of liquefiable layer (m)	H_2 (m)	H_1 (m)	$CSR_{7.5avg}$	$I_{c\ avg}$	$q_{C1N\ avg}$
WP24	3	3	0.40	5.90	**17.99**	***28.12***	**0.16**	3.5–8.7	5.2	3.5	0.21	1.91	47.89
Morelli1	1	3	0.45	6.10	**4.94**	***8.69***	***0.04***	3.7–5.2	1.5	3.7	0.23	2.56	22.95
Morelli2	1	3	0.46	6.10	**9.48**	***16.25***	**0.15**	3.0–6.0	3.0	3.0	0.23	2.44	38.32
Morelli3	1	3	0.45	6.10	**4.94**	***8.69***	***0.04***	3.7–5.2	1.5	3.7	0.23	2.56	22.95
Morelli4	1	3	0.45	6.10	**5.36**	***11.52***	**0.37**	3.1–5.3	2.2	3.1	0.22	2.60	21.38
WP09 XII Mor	1	3	0.45	6.10	**4.94**	***8.69***	***0.04***	3.7–5.2	1.5	3.7	0.23	2.56	22.95
WP12	1	3	0.45	6.10	**4.94**	***8.69***	***0.04***	3.7–5.2	1.5	3.7	0.23	2.56	22.95
Concordia 1	–	–	–	–	–	–	–	–	–	–	–	–	–
WP27_014	–	–	–	–	–	–	–	–	–	–	–	–	–
Ca 2	–	–	–	–	–	–	–	–	–	–	–	–	–
ca rossa 1	–	–	–	–	–	–	–	–	–	–	–	–	–
Fruttar_1	–	–	–	–	–	–	–	–	–	–	–	–	–
INS07	–	–	–	–	–	–	–	–	–	–	–	–	–
INS08	–	–	–	–	–	–	–	–	–	–	–	–	–
INS10	–	–	–	–	–	–	–	–	–	–	–	–	–
S.Mart1	–	–	–	–	–	–	–	–	–	–	–	–	–
San Martino1	–	–	–	–	–	–	–	–	–	–	–	–	–
San Martino 2a	–	–	–	–	–	–	–	–	–	–	–	–	–
San Martino 2b	–	–	–	–	–	–	–	–	–	–	–	–	–

Table 1 (continued)

Test site	Depth of in situ GWT (m)	Depth of earthquake GWT (m)	a_{max}	M_w	LPI	LSN	S(m)	Depth of liquefiable layer (m)	H_2 (m)	H_1 (m)	$CSR_{7.5avg}$	$I_{c\ avg}$	$q_{C1N\ avg}$
San Martino3	–	–	–	–	–	–	–	–	–	–	–	–	–
WP45	–	–	–	–	–	–	–	–	–	–	–	–	–
WP47 San Mar Spino	–	–	–	–	–	–	–	–	–	–	–	–	–
WP55	3	1	0.41	5.90	**17.13**	*20.73*	**0.15**	4.2–9.8	5.6	4.2	0.28	2.29	45.67
WP60	3	1	0.41	5.90	**24.70**	**30.00**	**0.23**	4.2–9.8	5.6	4.2	0.28	2.29	45.67
WP64	3	1	0.41	5.90	**24.70**	**30.00**	**0.23**	4.2–9.8	5.6	4.2	0.28	2.29	45.67
WP66	3	1	0.41	5.90	**24.70**	**30.00**	**0.23**	4.2–9.8	5.6	4.2	0.28	2.29	45.67
Moglia1	–	–	–	–	–	–	–	–	–	–	–	–	–
Reno1	1	1	0.42	6.10	*24.44*	*54.08*	**0.15**	1.0–6.0	5.00	1.0	0.28	2.07	42.26
Reno2	1	1	0.42	6.10	**18.17**	26.45	**0.11**	2.7–6.8	4.1	2.7	0.32	2.30	28.93
INS01	–	–	–	–	–	–	–	–	–	–	–	–	–
Quist1	–	–	–	–	–	–	–	–	–	–	–	–	–
Quist2	–	–	–	–	–	–	–	–	–	–	–	–	–
Quist3	–	–	–	–	–	–	–	–	–	–	–	–	–
Quist4	–	–	–	–	–	–	–	–	–	–	–	–	–
WPT073/AP16	–	–	–	–	–	–	–	–	–	–	–	–	–
WPT109/AP43	–	–	–	–	–	–	–	–	–	–	–	–	–
San Felice1	–	–	–	–	–	–	–	–	–	–	–	–	–

Table 1 (continued)

Test site	Depth of in situ GWT (m)	Depth of earthquake GWT (m)	a_{max}	M_w	LPI	LSN	S(m)	Depth of liquefiable layer (m)	H_2 (m)	H_1 (m)	$CSR_{7.5avg}$	$I_{c\ avg}$	$q_{C1N\ avg}$
San Felice2	–	–	–	–	–	–	–	–	–	–	–	–	–
San Felice3	–	–	–	–	–	–	–	–	–	–	–	–	–
San Felice4	–	–	–	–	–	–	–	–	–	–	–	–	–
San Felice5	–	–	–	–	–	–	–	–	–	–	–	–	–
San Felice7	–	–	–	–	–	–	–	–	–	–	–	–	–
San Felice8	–	–	–	–	–	–	–	–	–	–	–	–	–
WP01	–	–	–	–	–	–	–	–	–	–	–	–	–
WP02	–	–	–	–	–	–	–	–	–	–	–	–	–
WP04	–	–	–	–	–	–	–	–	–	–	–	–	–
WP08	–	–	–	–	–	–	–	–	–	–	–	–	–
WP09 San fel Stadio	–	–	–	–	–	–	–	–	–	–	–	–	–
WP15	–	–	–	–	–	–	–	–	–	–	–	–	–
WP18	–	–	–	–	–	–	–	–	–	–	–	–	–
WP27	–	–	–	–	–	–	–	–	–	–	–	–	–
WP29	–	–	–	–	–	–	–	–	–	–	–	–	–
WP34	–	–	–	–	–	–	–	–	–	–	–	–	–
WP40	–	–	–	–	–	–	–	–	–	–	–	–	–
INS02	–	–	–	–	–	–	–	–	–	–	–	–	–
Cast1	3	1	0.46	6.10	**21.47**	***26.41***	**0.30**	6.2–20.0	13.8	6.2	0.31	2.07	73.43
Casum1	3	1	0.46	6.10	**24.27**	***26.66***	**0.40**	5.8–20.0	14.2	5.8	0.31	1.85	83.42
Casum2	3	1	0.46	6.10	**24.27**	***26.66***	**0.40**	5.8–20.0	14.2	5.8	0.31	1.85	83.42

Table 1 (continued)

Test site	Depth of in situ GWT (m)	Depth of earthquake GWT (m)	a_{max}	M_w	LPI	LSN	S(m)	Depth of liquefiable layer (m)	H_2 (m)	H_1 (m)	$CSR_{7.5avg}$	$I_{c\ avg}$	$q_{C1N\ avg}$
fgmv064	3	1	0.46	6.10	**24.27**	***26.66***	**0.40**	5.8–20.0	14.2	5.8	0.31	1.85	83.42
Mirabello new	3	–	–	–	–	–	–	–	–	–	–	–	–
Mirabello1	3	–	–	–	–	–	–	–	–	–	–	–	–
Mirabello2	3	3	0.44	6.10	**10.07**	***12.17***	**0.18**	6.8–9.1	2.3	6.8	0.27	2.20	37.83
Mirabello3	3	–	–	–	–	–	–	–	–	–	–	–	–
WP36	3	1	0.46	6.10	**24.27**	***26.66***	**0.40**	5.8–20.0	14.2	5.8	0.31	1.85	83.42
WP47 San Car (upper)	3	1	0.46	6.10	*28.78*	*32.29*	*0.34*	4.2–20.0	15.8	4.2	0.30	2.12	66.83
WP47a San Car	3	1	0.46	6.10	*28.78*	*32.29*	*0.34*	4.2–20.0	15.8	4.2	0.30	2.12	66.83
S.Agost_11	1	3	0.46	6.10	**18.42**	***23.78***	**0.20**	3.2–9.1	5.9	3.2	0.25	2.31	33.57
S.Agost_12	1	3	0.46	6.10	**18.42**	***23.78***	**0.20**	3.2–9.1	5.9	3.2	0.25	2.31	33.57
San Carlo M_5	–	–	–	–	–	–	–	–	–	–	–	–	–
San Carlo new	1	–	–	–	–	–	–	–	–	–	–	–	–
San Carlo1	1	–	–	–	–	–	–	–	–	–	–	–	–
San Carlo2b	1	–	–	–	–	–	–	–	–	–	–	–	–
San Carlo3	1	–	–	–	–	–	–	–	–	–	–	–	–
San Carlo4	1	–	–	–	–	–	–	–	–	–	–	–	–
San Carlo5	–	–	–	–	–	–	–	–	–	–	–	–	–

Table 1 (continued)

Test site	Depth of in situ GWT (m)	Depth of earthquake GWT (m)	a_{max}	M_w	LPI	LSN	S(m)	Depth of liquefiable layer (m)	H_2 (m)	H_1 (m)	$CSR_{7.5avg}$	$I_{c\ avg}$	$q_{C1N\ avg}$
San Carlo6	–	–	–	–	–	–	–	–	–	–	–	–	–
San Carlo7	1	1	0.46	6.10	*18.88*	**30.49**	*0.27*	1.5–7.2	5.7	1.5	0.32	2.40	35.61
Tosatti 3	–	–	–	–	–	–	–	–	–	–	–	–	–
WP49 san car	1	1	0.46	6.10	**21.82**	**30.49**	**0.14**	2.9–6.7	3.8	2.9	0.35	2.04	40.01
WP49(2)	1	1	0.46	6.10	**21.82**	**30.49**	**0.14**	2.9–6.7	3.8	2.9	0.35	2.04	40.01
WP57	1	–	–	–	–	–	–	–	–	–	–	–	–
WP63	1	1	0.46	6.10	**23.56**	**42.39**	**0.27**	1.0–6.3	5.3	1.0	0.31	2.05	46.78
WP68	–	–	–	–	–	–	–	–	–	–	–	–	–
WP79	1	–	–	–	–	–	–	–	–	–	–	–	–
WP82	1	–	–	–	–	–	–	–	–	–	–	–	–
Tortiola1	3	3	0.44	6.10	**27.86**	**39.43**	**0.35**	3.0–19.0	16.0	3.0	0.25	2.08	57.72
Tortiola2	3	3	0.45	6.10	**28.59**	**40.00**	**0.35**	3.0–19.0	16.0	3.0	0.25	2.08	57.72

FC = fines content; U = coefficient of uniformity; C = coefficient of curvature; σ = sorting; Liquefaction-induced land damage categories (see section 3.1, van Ballegooy et al. 2014); a_{max} = peak ground acceleration; M_w = moment magnitude; LPI = liquefaction potential index, LSN = liquefaction severity number, S = vertical settlement. The text formatting is used to describe the accuracy of the LPI, LSN and S approaches relative to the observed damage, namely: bold-italics is underpredicted, italics is overpredicted, bold is reasonable; H_1 = thickness of surface laye, H_2 = thickness of liquefiable layer; $CSR_{7.5\ avg}$ = average cyclic stress ratio for a M_w 7.5 earthquake; $I_{c\ avg}$ = average soil behavior type index; $q_{c1N\ avg}$ = average normalized overburden corrected cone tip resistance

$$\sigma = \frac{\phi_{84} - \phi_{16}}{4} + \frac{\phi_{95} - \phi_{5}}{4} \tag{3}$$

where $\phi_x = Log_2 D_x$ and D_x is the diameter of the generic xth percentile of the grain size curve in millimeters.

The grain size curves and the calculated index properties were then used to determine the Unified Soil Classification System symbols (USCS classification, ASTM D2487-11 2011) reported in Table 1. Sand boils were most frequently classified as silty sand (SM) and sometimes as poorly graded sand with silt (SP-SM) or sandy silt (ML), considering that FC varies on average between 10 and 40%, U is typically below 30 and C varies between 1 and 4.

The coarser samples (from medium sand to fine sand) are from sand blows in the northern area, between Bondeno and Quistello (see Fig. 1 for the their location), that is dominated by the Po River paleochannels. The sand blows from the eastern sector, dominated by the Reno paleochannel between Sant'Agostino and Mirabello (see Fig. 1 for the their location), are generally finer grained compared to those of the northern sector, and show a larger spectrum from fine-grained sands to silty sands. The samples from the western area (San Felice sul Panaro, Concordia sulla Secchia and Cavezzo) are characterized by the largest percentage of fines (up to 50%) and consist of fine-grained silty sands and sandy silts. These sands were ejected in the area dominated by the Secchia and Panaro rivers.

The grain size ranges for the four main fluvial systems (Po, Reno, Secchia and Panaro) are outlined in Fig. 4, showing that the Secchia and Panaro river sands are generally finer compared to the Po sediments, while the Reno deposits cover a wider grain-size range. Figure 4 indicates also that the liquefied sediments are within the grain size range of deposits typically susceptible to liquefaction according to observations of Tsuchida and Hayashi (1971). As shown in Fig. 5a, sorting of ejected sand is moderate to poor for all of the source rivers and the lowest degree of sorting generally characterizes the samples with higher fines content (Fig. 5b).

4.1.2 Petrographic composition analyses

Sand blows and dikes have a variable composition ranging from (1) lithoarenite to (2) quartz-rich lithoarenite and (3) quartzarenite (Fig. 6). The lithoarenitic sands contain an abundant lithic association including sedimentary fine-grained siliciclastic grains (siltstones and shales) and carbonate lithics (largely micritic limestones and calcite spars). Shales are well lithified, well rounded, with an evident iso-orientation of the clay minerals, and for these characters, they appear to have a detrital origin, derived from the erosion of the pelitic successions of various age cropping out in the northern Apennines. Serpentinite and volcanite grains are minor components. These petrofacies characterize the western area, dominated by the Secchia River paleochannels, near Mirandola, Cavezzo and Concordia sulla Secchia, but indicate an input of the Panaro River in the San Felice sul Panaro area. The quartz-rich lithoarenites show a higher quartz-feldspar content and a lower content of siltstones, shales and carbonate lithics. This petrofacies typifies the samples from the eastern sector attributable to the Reno River paleochannels in the area between San Carlo and Mirabello. The quartzarenite sands are characterized by a significantly higher content of quartz and feldspar grains associated with metamorphic rock fragments, abundant micas and heavy minerals. These latter samples are attributable to the Po River paleochannels in the northern sector of the plain.

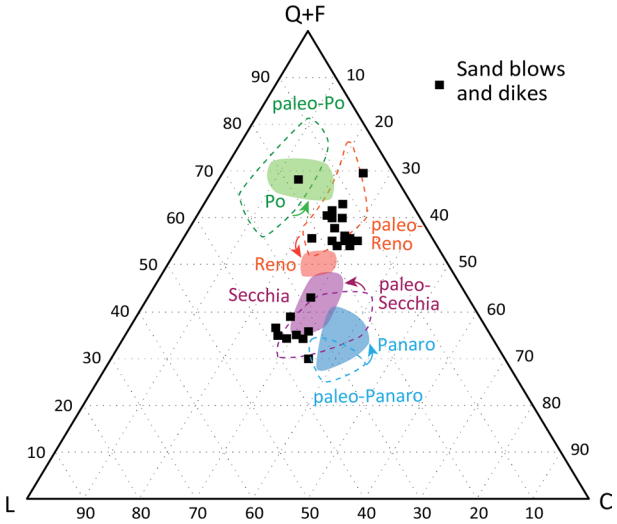

Fig. 6 Q+F, L, C diagram showing the composition of sands from sand blows and dikes (black squares). The compositional fields of modern and paleoriver of the Emilia plain are also reported (Lugli et al. 2007). Q: quartz; F: feldspars; L: siliciclastic rock fragments; C: carbonate rock fragments

4.2 Geotechnical characterization of liquefied sites

4.2.1 In situ tests

The great majority of the in situ tests presented in this work consist of CPTUs and CPTEs that are plotted in each sheet of the 56 analyzed sites, where in situ tests are available (supplement of this paper), in terms of: corrected cone resistance (q_t), sleeve friction (f_s), pore pressure (u_2, only for CPTU) and soil behavior type index (I_c), according to Robertson (2004). This allowed a preliminary subsoil interpretation identifying the depth of the in situ ground water table, defined as "Depth of in situ GWT" in Table 1, and the "sand-like" layers associated with $I_c \leq 2.6$ (Idriss and Boulanger 2008). As an example, Fig. 7 provides the CPTU results collected at the WP63 test site, located in San Carlo (municipality of Terre del Reno). The upper 6 m depth are composed by silty sands and sandy silts (approximately $I_c \leq 2.6$), while a thick silty-clayey layer is encountered up to 22 m depth ($I_c > 2.6$). A sandy body is then detected between 23 and 27 m, and finally clayey deposits can be found up to 30 m. This information, coupled with the u_2 profile, makes it possible to interpret the depth of the in situ GWT, which is approximately one meter below the ground surface.

Moreover, when available the sheets for each area (see supplement of this paper) include the DMTs and SDMTs geotechnical parameters according to Marchetti et al. (2001), including: the material index (I_D), the constrained modulus (M), the undrained shear strength (s_u), the horizontal stress index (K_D) and the shear wave velocity (V_S) from seismic dilatometer (SDMT) testing. Finally, when boreholes and standard penetration tests (SPT) are available, each sheet also plots an interpreted borehole log and the SPT blow count (N_{SPT}). Altogether, this information supports the geotechnical characterization of the liquefied sites.

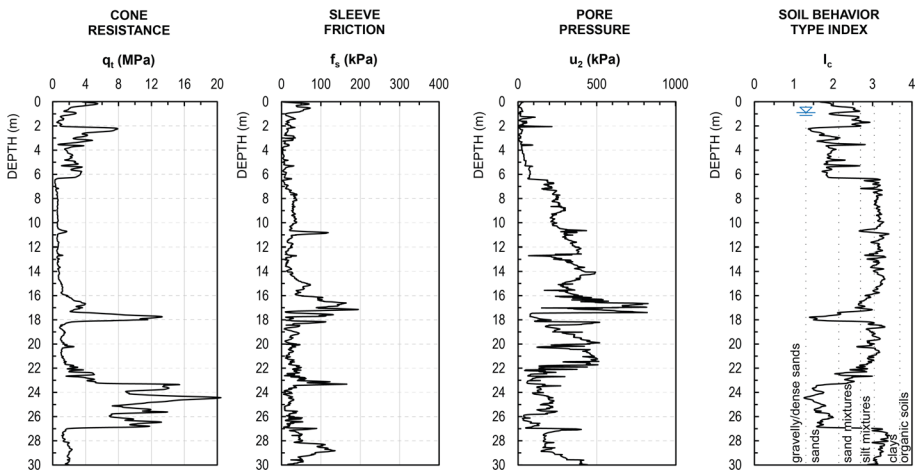

Fig. 7 Example of CPTU test results at WP63 San Carlo–Terre del Reno site

4.2.2 Liquefaction assessment

At each liquefied test site, where in situ tests were available and lateral spreading was not observed (45 sites, see Table 1), liquefaction susceptibility analyses were carried out using CPT- or DMT-based methods derived from the Seed and Idriss (1971) simplified procedure with the final goal of detecting the liquefied layer(s) for the 2012 earthquakes. The test sites located approximately east of San Felice sul Panaro were associated with the mainshock that occurred on the 20th May 2012, while the liquefied sites west of San Felice sul Panaro were coupled with the 29th May 2012 earthquake (Pizzi and Scisciani 2012).

For the definition of the peak ground acceleration (a_{max}) we used the most updated ground motion model for shallow crustal earthquakes in Italy (ITA18, Lanzano et al. 2019). This ground-motion prediction equation accounts for the more recent earthquakes that have occurred in Italy, including the 2012 Emilia earthquakes, and it is calibrated by regression of empirical ground-motion amplitudes against a set of predictor variables such as earthquake magnitude, focal mechanism, source-to-site distances, and local soil conditions (i.e. the time-averaged shear wave velocity to 30 m depth). Figure 8 compares the a_{max} from ITA18 with both the recorded data, acquired during the May 20th and the May 29th mainshocks, and the computed ShakeMaps (http://shakemap.rm.ingv.it/shake4, last access Oct. 22th, 2021; Michelini et al. 2020). The lack of seismic stations in the 2012 epicentral area during the 20th May 2012 mainshock (only one permanent station was located in the area, in the municipality of Mirandola; Cultrera et al. 2014) resulted in unreliable ShakeMap estimates in the near source region (Fig. 8a), as already noted by Cultera et al. (2014). The 29th May ShakeMap values are better constrained because of the large number of temporary seismic stations installed in the epicentral area (Fig. 8b), and they range within one standard deviation of the ground motion model prediction. We are then confident about using the ITA18 prediction for both earthquakes, with a careful choice of the input parameters, such as the M_w and the distance metrics.

Moment magnitude (M_w) of 6.1 and 5.9 are computed by Pondrelli et al. (2012) by means of the Regional Centroid-Moment Tensors (RCMT, http://rcmt2.bo.ingv.it/, last access: October 2021; Pondrelli 2002). The M_w estimates from RCMT are equivalent to

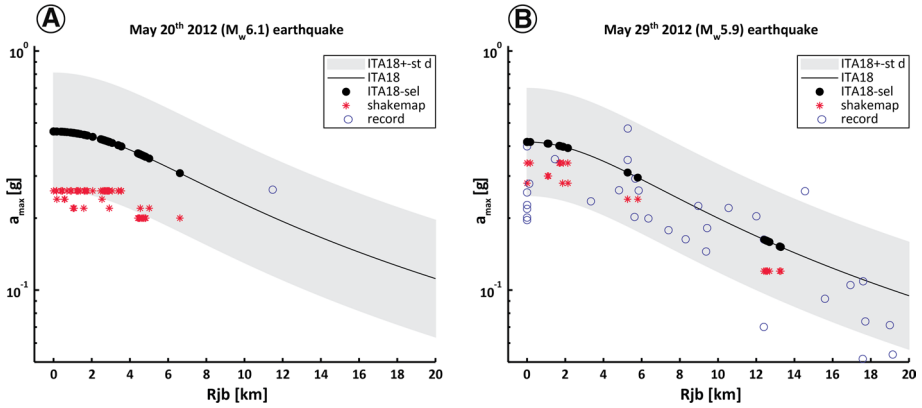

Fig. 8 Peak ground acceleration (a_{max}) recorded and modeled for the 2012 Emilia earthquakes, as a function of the Joyner-Boore distance (Rjb): (**a**) M_w 6.1 on May 20th, (**b**) M_w 5.9 on May 29th. a_{max} of ITA18 is the median of orientation independent amplitudes (Lanzano et al. 2019)

the global scale solutions of the Global Centroid Moment Tensors project (GCMT, http://www.globalcmt.org, Ekström et al. 2012), which is considered the most authoritative agency for M_w of earthquakes worldwide and whose magnitudes are used as a reference in many seismological studies (Di Giacomo et al. 2021). Moreover, both estimates almost overlap for $M_w > 5.4$ (Gasperini et al. 2012).

Regarding the distance metrics, we used the Joyner-Boore distance (Rjb) to account for the effect of the extended source in ITA18, as the sites analyzed in this study are very close to the seismic sources of the mainshocks. The fault geometries, reported in Fig. 1, are taken from the available literature and limited to the area with source slip greater than 0 m: Pezzo et al. (2018) for the M_w 6.1 on May 20th and Paolucci et al. (2015) for the M_w 5.9 on May 29th.

As a consequence, the cyclic stress ratio for a M_w 7.5 earthquake ($CSR_{7.5}$) was evaluated using the previously noted mainshock values of M_w and a_{max}. The present research is limited to reproducing the liquefaction evidence induced by the mainshoks of May 20th and May 29th using the simplified procedure. Reproduction of the possible additional liquefaction effects that occurred in conjunction with the aftershocks within the first four minutes after the mainshock of May 20th would have necessitated numerical modelling to reproduce the entire pore pressure build up (i.e. from the starting time of the mainshock to at least few minutes after the last strong aftershock here considered). The performance of numerical modelling for the numerous sites analyzed in the manuscript would have required: (1) a large number of seismic recording stations in the epicentral area of the 20th May 2012 mainshock; and (2) substantially more geotechnical information extending down to the bedrock. Unfortunately, these data are not available in the literature due to the lack of seismic stations (only the Mirandola station recorded the seismic event, see Cultrera et al. 2014) and due to the presence of deep bedrock (> 100 m in the anticlinal area of Mirandola and Casaglia, and >> 300 m in the synclinal areas that cover most of the epicentral area, see Martelli 2021, Minarelli et al. 2016).

Additionally, the magnitude scaling factor (MSF) and the shear stress reduction coefficient (r_d) were evaluated according to the equations recommended by Idriss and Boulanger (2008) for CPT, DMT and CPT-DMT methods, while the depth of the earthquake ground

water table, defined as "Depth of earthquake GWT" in Table 1, was assumed equal to 3 m depth in the case of a fluvial ridge and to 1 m in the case of a flat interfluvial depression, considering that the geomorphological features of the study area based on LIDAR data (Table 1).

Finally, the cyclic resistance ratio (CRR) for a M_w 7.5 earthquake ($CRR_{7.5}$) was evaluated using (1) the normalized overburden corrected cone tip resistance q_{c1N} calculated from the Idriss and Boulanger (2008) CPT-based method; (2) the horizontal stress index K_D estimated from Marchetti (2016) with DMT methods; and (3) the combination of q_{c1N} and K_D parameters in the Marchetti (2016) CPT-DMT correlation. The ratio between $CRR_{7.5}$ and $CSR_{7.5}$ defines the safety factor against liquefaction (FS_{liq}). To screen out "clay-like" soils, a threshold was set at $I_c \leq 2.6$ for CPT data and at $I_D \geq 1.0$ for DMT measurements. Liquefaction severity indexes were also calculated for CPT profiles in terms of:

- the liquefaction potential index (LPI) proposed by Iwasaki et al. (1982), given by the equation:

$$LPI = \int_0^{20} F(z) \cdot w(z) \cdot dz \tag{4}$$

  where $w(z) = 10 - 0.5 \cdot z$, $F(z) = 1 - FS_{liq}$ if $FS_{liq} \leq$ or $F(z) = 0$ if $FS_{liq} > 1$, and z is the depth below the ground surface;
- the liquefaction induced vertical settlements (S) according to Zhang et al. (2002), given by the equation:

$$S = \sum_{i=1}^{j} \varepsilon_{vi} \cdot \Delta z_i \tag{5}$$

  where ε_{vi} is the post liquefaction volumetric strain, calculated as a function of the liquefaction safety factor (FS_{liq}) and of the equivalent clean sand normalized CPT penetration resistance $(q_{c1N})_{cs}$, Δz_i is the thickness of the sublayer i, and j is the number of soil sublayers;
- the liquefaction severity number (LSN) proposed by van Ballegooy et al. (2014), given by the equation:

$$LSN = 1000 \cdot \int \frac{\varepsilon_v}{z} \cdot dz \tag{6}$$

where ε_v is the post liquefaction volumetric strain calculated according to Zhang et al. (2002).

The predictive indexes were computed to verify how well they fit the experimental evidence of the 2012 Emilia seismic sequence. As an example, Fig. 9 reports the results of the CPTU liquefaction analysis performed at the WP63 San Carlo site for the seismic event of the 20th May 2012 ($M_w = 6.1$). A surface non-liquefiable layer with a thickness $H_1 = 1.0$ m and a liquefiable layer of a thickness $H_2 = 5.3$ m (depth range: 1.0–6.3 m) are detected with associated LPI = 23.56, LSN = 42.39 and S = 0.27 m. By looking at the observed liquefaction evidences through the identified liquefaction-induced land damage categories (see Table 1), the liquefaction severity indexes (LPI, LSN and S) results in reasonable agreement with the 2012 effects on ground surface, classified in Category 4 (i.e. no lateral spreading but large quantities of ejected material). Reasonable agreement is noted for

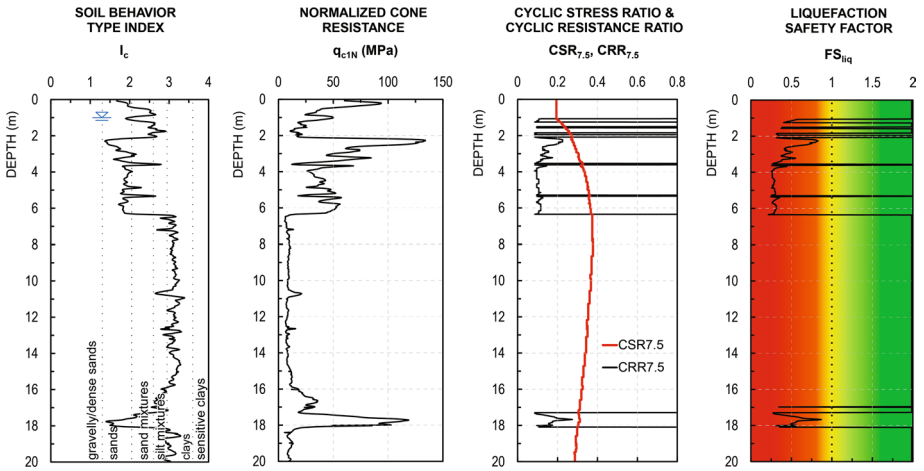

Fig. 9 Example of CPTU liquefaction analysis at WP63 San Carlo–Terre del Reno site for the seismic event of the 20th May 2012 ($M_w = 6.1$)

approximately the 75% of the analyzed cases, in terms of LPI and S, while for the remaining percentage the liquefaction prediction results underestimated or overestimated. The LSN provides reasonable agreement with the observed performance for less than the 40% of the analyzed liquefied sites, while for the majority of cases this index underpredicted the field observations. This is likely because the LSN threshold values corresponding to different severities of liquefaction are based on the New Zealand data. Further details can be detected in Table 1 where the text formatting is used to describe the accuracy of the LPI, LSN and S approaches relative to the observed damage, namely: bold-italics is underpredicted, italics is overpredicted, bold is reasonable.

5 Liquefaction features versus depositional facies and sediment provenance

The composition of ejected sand is a fundamental tool for the source layer identification in a sedimentary sequence, and this is pivotal for the recognition of potential areas prone to hazardous sand liquefaction phenomena. On the other hand, the petrographic composition does not necessarily appear to be a significant factor influencing the liquefaction susceptibility, as demonstrated by the wide compositional spectrum of the Po plain alluvial systems illustrated in this study.

As noted previously, the stratigraphic architecture of the study area is strongly influenced by the interaction between the Po River and the network of transversal tributaries draining the Apennine chain (Fig. 10). The post-glacial Po River deposits consist of elongated channel sand bodies, with quartzarenitic composition representing detritus from wide sectors of the Alpine and Apennine chains, transported over a long distance. The Apennine sands are confined in narrow channel body, and are finer grained, containing a larger amount of silt. They show lower quartz-feldspar contents and abundant sedimentary lithics derived from relatively smaller catchments confined to the external belts of the chain; detritus is derived only from the sedimentary cover.

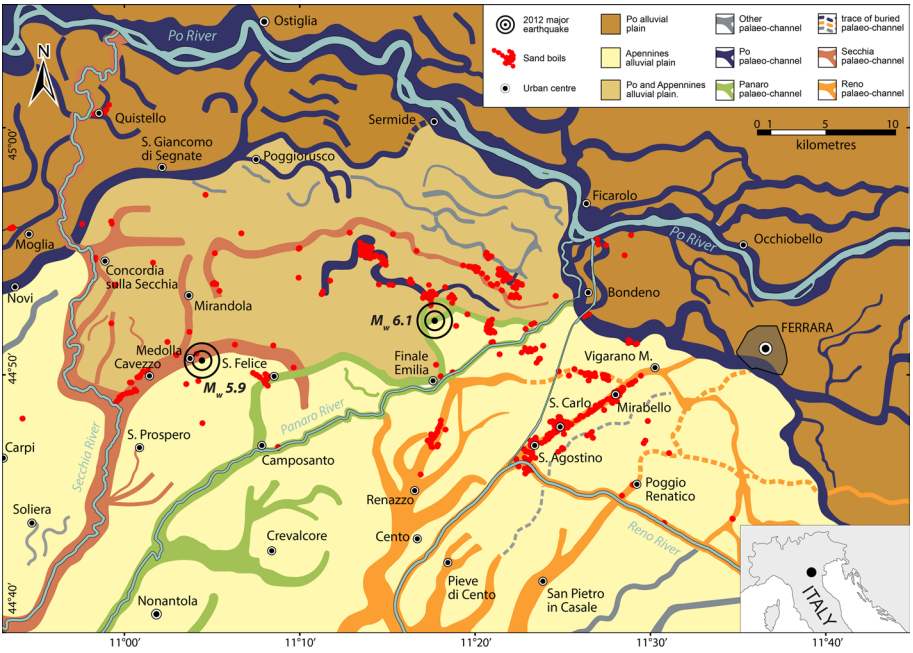

Fig. 10 Main fluvial domains of the study area and paleochannel sand bodies in the shallow subsurface (modified from Stefani et al. 2018). Liquefaction sites are aligned along paleochannels as also reported by Civico et al.(2015)

A distinctive sand composition characterizes each river mainly based on the prevailing lithic grains. Sediments eroded from shale terrains with carbonate blocks (the chaotic Ligurian units) dominate the Secchia and Panaro catchments (litharenitic petrofacies). These lithic components are less abundant in the Reno River (quartz-rich lithoarenite petrofacies). Sand petrography data demonstrate that fluvial sand compositions have slightly varied during the Holocene with respect to the present-day sands, as shown by the compositional fields of Fig. 6. This is particularly evident for the modern Reno River sands, which are more litharenitic compared to its paleochannel. The Po River sands are richer in quartz, feldspar, and metamorphic grains.

The petrography of the sand blows therefore makes it possible to discriminate the sedimentary provenance of the sand ejected during the 2012 seismic crisis and to ascribe them to their respective Po, Secchia and Reno Holocene paleochannels (Fig. 10). The petrography of sands has also supported the identification of the source level of liquefaction, in all sites located at depth between 5 and 8 m in the alluvial sediment sequence.

This comprehensive dataset shows that earthquake-induced liquefaction phenomena affected sand layers with significant contents of non-plastic silt and was not limited to clean sands and well-sorted deposits, as suggested by previous results from Fontana et al. (2015, 2019) and Amoroso et al. (2020). Within the considered alluvial plain, liquefaction primarily affects silty sand with litharenitic composition from laterally confined depositional bodies, such as levee, crevasse splay, to minor channel ribbons. Subordinately liquefaction was related to thick channel-fill sands deposited by the Po river.

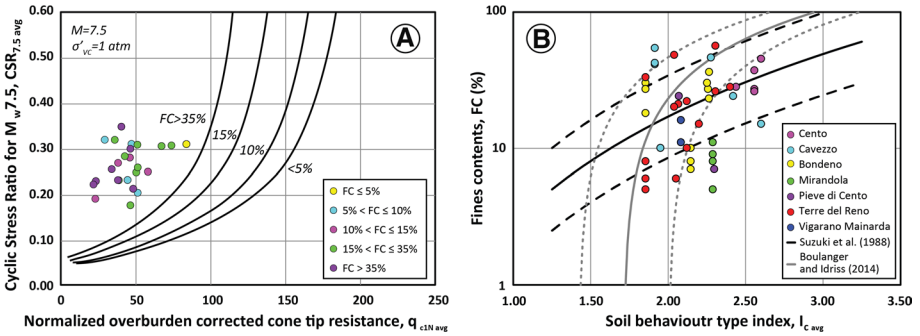

Fig. 11 Summary liquefaction charts for the analyzed test sites: (**a**) liquefaction triggering curves by Idriss and Boulanger (2008), (**b**) fines content correlations by Suzuki et al. (1998) and Boulanger and Idriss (2014). Dashed lines indicates the upper and lower boundaries of the two curves

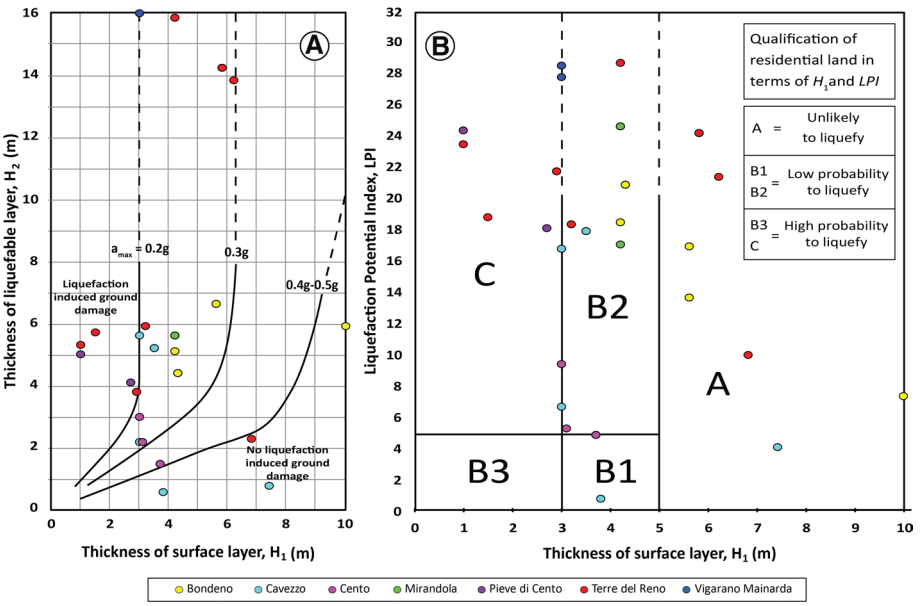

Fig. 12 Summary liquefaction charts involving the surface non-liquefiable layer for the analyzed test sites: (**a**) Ishihara (1985) chart and (**b**) Towhata et al. (2016) chart. Dashed lines represent a possible extension of the two charts to fit the experimental data

6 Liquefaction charts

The liquefied layers identified at the trial sites (Table 1) were subsequently used to develop summary liquefaction charts, as reported in Figs. 11 and 12. In particular, Fig. 11a compares the average $CSR_{7.5}$ ($CSR_{7.5\ avg}$) and average q_{c1N} ($q_{c1N\ avg}$) within each identified liquefied layer, with the CPT-based liquefaction triggering curves by Idriss and Boulanger (2008). The average parameters (i.e. $CSR_{7.5\ avg}$ and $q_{c1N\ avg}$) were calculated using

the $CSR_{7.5}$ and q_{c1N} values for the entire liquefied layer thickness. The liquefaction data points for the entire dataset are consistent with the Idriss and Boulanger (2008) triggering curves which indicate liquefaction in all cases, even though the plot provides $CSR_{7.5\ avg}$ and $q_{c1N\ avg}$ pairs for the entire liquefied layer at each site, rather than the "critical layer" computed with the lowest average $q_{c1Ncs}/CSR_{7.5}$ ratio (where q_{c1Ncs} is the normalized cone tip resistance for clean sand) over a depth range of about a meter. The identification of the critical layer at each site would have produced $q_{c1N\ avg}$ values somewhat smaller (less than 38%) with little effect on the $CSR_{7.5\ avg}$ (less than 9%), but the results would still plot above the liquefaction triggering curves for all the data points indicating agreement with the observed behavior.

Figure 11b plots the FC from the sand boil samples versus the average I_c ($I_{c\ avg}$) estimated from the 2012 liquefied layer in comparison with correlations by Suzuki et al. (1998) and by Boulanger and Idriss (2014). The FC and $I_{c\ avg}$ data pairs exhibit considerable scatter for a significant number of case studies relative to the average curves provided by Suzuki et al. (1998) and Boulanger and Idriss (2014) (Fig. 11b), although less than the 35–40% of the cases plot outside the upper and lower boundary curves. This scatter may be related to a site-specific dependency of these kind of I_c-FC correlations (Idriss and Boulanger 2008; Boulanger and Idriss 2014) and to the fact that I_c can be seen as a parameter related to the mechanical soil response, including soil plasticity, and not strictly to the grain size of the soil deposits alone (Robertson and Cabal 2015).

Finally, Fig. 12 evaluates liquefaction manifestation at the ground surface relative to the presence of a non-liquefiable surface crust if thickness H_1 overlying a liquefiable deposit of thickness H_2 according to charts developed by Ishihara (1985) and by Towhata et al. (2016) using H_1 and LPI. Almost the 90% of the experimental liquefaction observations correctly fit with Ishihara chart (Fig. 12a), considering the range of peak ground accelerations used in the liquefaction assessment ($a_{max} = 0.40$–0.46g, see also Table 1). In only four cases, related to the municipalities of Bondeno, Cavezzo and Terre del Reno, does the chart incorrectly predict that liquefaction would not be observed at the ground surface probably due to the presence of a thick non-liquefiable crust ($H_1 \approx 4$–10 m). The prediction provided by the Towhata chart (Fig. 12b) is far less accurate and contemplates highly probable surface manifestations of liquefaction for less than 25% of the analyzed cases. In this respect, for the analyzed Emilia dataset the chart proposed by Ishihara (1985) looks to provide more reliable results using the H_1-H_2 pairs than the one proposed by Towhata et al. (2016) where the non-liquefiable crust is coupled with the LPI in place of H_2.

7 Conclusions

We have compiled a large and comprehensive dataset consisting of 120 liquefied sites induced by the 2012 Emilia Romagna earthquakes in the alluvial plain created by the late Quaternary sedimentation of Apennine fluvial systems and of the Po River. This compilation includes the entire available structural, grain size, compositional and geotechnical data for each liquefaction site consisting of a wide spectrum of sediment types.

A strong relationship exists between the occurrence of liquefaction and the stratigraphic architecture of the subsurface. The granular sediments ejected to the surface are entirely derived from Holocene units, associated with river channel, levee, and crevasse deposits. The geometry of the fluvial paleochannels contributed to confine the liquefaction sites along narrow ribbons crossing the plain. In addition, coseismic surface

fractures were largely localized across fluvial ridge morphologies. The source level for liquefaction in all sites was identified at shallow depth, in sand layers, mainly between 3 and 6 m, covered by fine-grained cohesive deposits. The granular sediments involved in the liquefaction phenomena often show a significant amount of non-plastic silt. The texture and composition of sand blows has allowed us to identify the provenance of the sand ejected and to ascribe them to their respective fluvial channel. The sands deposited by the Po River are organized in large, vertically stacked channel bodies with quartzarenitic composition, whereas the Apennine drainage systems generated narrower channel bodies rich in finer grained litharenitic sands and silty sands.

The availability of in situ tests at the liquefied sites allows us to verify and validate the reliability of the liquefaction charts in alluvial sediments. In this respect, the comparisons of the liquefaction severity indexes with the coseismic observations revealed that the LPI and S generally is consistent with the 2012 evidences while the LSN seems to underestimate the surface manifestation of liquefaction probably due to the dependency of LSN on the New Zealand dataset for which it has been developed.

The CPT data points at the liquefied sites fit well with the triggering chart developed by Idriss and Boulanger (2008), highlighting the consistency of this simplified method for evaluating liquefaction. In contrast, the I_c-FC correlations by both Suzuki et al. (1998) and Boulanger and Idriss (2014) only provide a broad estimate of the true fines contents of the 2012 sand ejecta (as measured by the grain size analyses), although 60–65% of measured fines content from sand boils at liquefaction sites fall within the upper and lower boundary curves. The dispersion of these data points around the average curves denotes the site-specific nature of I_c-FC correlations and the effect of plasticity and mechanical behavior associated with I_c rather than simply the grain size.

For the vast majority of the data points (almost the 90% of the analyzed cases) for the Emilia earthquakes, the presence of a medium-thick non-liquefiable crust (≈ 3–6 m thick) related to the range of the 2012 peak ground accelerations ($a_{max} = 0.40–0.46g$) did not prevent surface manifestations of liquefaction in agreement with the liquefaction charts proposed by Ishihara (1985). In contrast, the Towhata et al. (2016) chart only predicted surface liquefaction features for a small percentage of the dataset (less than 25% of the analyzed cases) where liquefaction actually occurred. Therefore, for the analyzed Emilia case studies the use of non-liquefiable crust provides better estimations of the liquefaction manifestations when coupled with the thickness of the liquefiable layer (H_2) rather than with the liquefaction potential index (LPI). These coseismic liquefaction observations emphasize the importance of an in-depth study of geological and geotechnical properties of these crusts.

Supplementary Information The online version contains supplementary material available at https://doi.org/10.1007/s10518-022-01338-7.

Acknowledgements Special thanks to GeoLogismiki to freely provide the CLiq software to run the liquefaction analyses, to Emanuele Della Morte, to Davide Franciosi and to Francesco Di Buccio to support the development of the liquefaction database, to Alessandro Fontana to provide the RADAR images of Po plain, to Alessandra Smedile and Stefania Pinzi to collect and analyze a part of the sand boil samples. This work is also part of a research project funded by ReLUIS (University Network of Seismic Engineering Laboratories) Consortium 2019-2021, WP 16 Geotechnical Engineering, Task 16.1 Site response and liquefaction and by Search for Excellence – UdA 2019 (University of Chieti-Pescara), Evaluation and Improvement of Methods to Consider Influence of Surface Clay Layers on Liquefaction-Induced Settlement (CLIQUEST).

Funding This work is partly funded by ReLUIS (University Network of Seismic Engineering Laboratories) Consortium 2019-2021, WP 16 Geotechnical Engineering, Task 16.1 Site response and liquefaction and by Search for Excellence – UdA 2019 (University of Chieti-Pescara), Evaluation and Improvement of

Methods to Consider Influence of Surface Clay Layers on Liquefaction-Induced Settlement (CLIQUEST). However, the opinions, conclusions, and recommendations in this paper do not necessarily represent those of the sponsors.

Declarations

Conflict of interest The authors declare no competing interests.

References

Amoroso S, Milana G, Rollins KM, Comina C, Minarelli L, Manuel MR, Monaco P, Franceschini M, Anzidei M, Lusvardi C, Cantore L, Carpena A, Casadei S, Cinti FR, Civico R, Cox BR, De Martini PM, Di Giulio G, Di Naccio D, Di Stefano G, Facciorusso J, Famiani D, Fiorelli F, Fontana D, Foti S, Madiai C, Marangoni V, Marchetti D, Marchetti SL, Martelli L, Mariotti M, Muscolino E, Pancaldi D, Pantosti D, Passeri F, Pesci A, Romeo G, Sapia V, Smedile A, Stefani M, Tarabusi G, Teza G, Vassallo M, Villani F (2017) The first Italian blast-induced liquefaction test (Mirabello, Emilia-Romagna, Italy): description of the experiment and preliminary results. Ann Geophys 60(5):S0556. https://doi.org/10.4401/ag-7415

Amoroso S, Rollins KM, Andersen P, Gottardi G, Tonni L, García Martínez MF, Wissmann KJ, Minarelli L, Comina C, Fontana D, De Martini PM, Monaco P, Pesci A, Sapia V, Vassallo M, Anzidei M, Carpena A, Cinti F, Civico R, Coco I, Conforti D, Doumaz F, Giannattasio F, Di Giulio G, Foti S, Loddo F, Lugli S, Manuel MR, Marchetti D, Mariotti M, Materni V, Metcalfe B, Milana G, Pantosti D, Pesce A, Salocchi AC, Smedile A, Stefani M, Tarabusi G, Teza G (2020) Blast-induced liquefaction in silty sands for full-scale testing of ground improvement methods: insights from a multidisciplinary study. Eng Geol 265:105437. https://doi.org/10.1016/j.enggeo.2019.105437

Andrus RD, Stokoe KH II (2000) Liquefaction resistance of soils from shear-wave velocity. J Geotech Geoenviron Eng 126(11):1015–1025. https://doi.org/10.1061/(ASCE)1090-0241(2000)126:11(1015)

ASTM D2487–11 (2011) Standard Practice for Classification of Soils for Engineering Purposes (Unified Soil Classification System). ASTM International, West Conshohocken, PA

Boulanger RW, Idriss IM (2014) CPT and SPT based liquefaction triggering procedures. Rep No UCD/CGM-14/01. Davis C A: Center for Geotechnical Modeling, Dept of Civil and Environmental

Cao Z, Youd TL, Yuan X (2011) Gravelly soils that liquefied during 2008 Wenchuan, China earthquake, Ms=8.0. Soil Dyn Earth Eng 31:1132–1143

Caputo R, Papathanasiou G (2012) Ground failure and liquefaction phenomena triggered by the 20 May, 2012 Emilia-Romagna (Northern Italy) earthquake: case study of Sant'Agostino – San Carlo - Mirabello zone. Nat Hazards Earth Syst Sci 12(11):3177–3180. https://doi.org/10.5194/nhess-12-3177-2012

Caputo R, Poli ME, Minarelli L, Rapti D, Sboras S, Stefani M, Zanferrari A (2016) Palaeoseismological evidence for the 1570 Ferrara earthquake. Italy Tecton 35(2):1423–1445. https://doi.org/10.1002/2016TC004238

Cetin KO, Seed RB, Der Kiureghian A, Tokimatsu K (2004) Standard penetration test-based probabilistic and deterministic assessment of seismic soil liquefaction potential. J Geotech Geoenviron Eng 130(12):1314–1340. https://doi.org/10.1061/(ASCE)1090-0241(2004)

Civico R, Brunori CA, De Martini PM, Pucci S, Cinti FR, Pantosti D (2015) Liquefaction susceptibility assessment in fluvial plains using airborne LIDAR: the case of the 2012 Emilia earthquake sequence area (Italy). Nat Hazards Earth Syst Sci 15:2473–2483

Cultrera G, Faenza L, Meletti C, D'Amico V, Michelini A (2014) Amato A (2014) Shakemaps uncertainties and their effects in the post-seismic actions for the 2012 Emilia (Italy) earthquakes. Bull Earthq Eng 12:2147–2164. https://doi.org/10.1007/s10518-013-9577-6

Di Giacomo D, Harris J, Storchak DA (2021) Complementing regional moment magnitudes to GCMT: a perspective from the rebuilt international seismological centre bulletin. Earth Syst Sci Data 13:1957–1985. https://doi.org/10.5194/essd-13-1957-2021

Ekström G, Nettles M, Dziewoński AM (2012) The global CMT project 2004–2010: centroid-moment tensors for 13,017 earthquakes. Phys Earth Planet in 200–201:1–9. https://doi.org/10.1016/j.pepi.2012.04.002

Emergeo Working Group (2012) A photographic dataset of the coseismic geological effects induced on the environment by the 2012 Emilia (northern Italy) earthquake sequence. Miscellanea INGV 16

Emergeo Working Group (2013) Liquefaction phenomena associated with the Emilia earthquake sequence of May-June 2012 (Northern Italy). Nat Hazards Earth Syst Sci 13(4):935–947

Facciorusso J, Madiai C, Vannucchi G (2015) CPT-based liquefaction case history from the 2012 Emilia earthquake in Italy. J Geotech Geoenviron Eng 141(12):1032–1051. https://doi.org/10.1061/(ASCE)GT.1943-5606.0001349

Facciorusso J, Madiai C, Vannucchi G (2016) The 2012 Emilia earthquake (Italy): geotechnical characterization and ground response analyses of the paleo-Reno river levees. Soil Dyn Earthq Eng 86:71–88. https://doi.org/10.1016/j.soildyn.2016.04.017

Folk RL, Ward WC (1957) Brazos River bar: a study in the significance of grain size parameters. J Sediment Petrol 27:3–26

Fontana D, Amoroso S, Minarelli L, Stefani M (2019) Sand liquefaction phenomena induced by a blast test: new insights from composition and texture of sands (late Quaternary, Emilia, Italy). J Sediment Res 89(1):13–27. https://doi.org/10.2110/jsr.2019.1

Fontana D, Lugli S, Marchetti Dori S, Caputo R, Stefani M (2015) Sedimentology and composition of sands injected during the seismic crisis of May 2012 (Emilia, Italy): clues for source layer identification and liquefaction regime. Sediment Geol 325:158–167

Gasperini P, Lolli B, Vannucci G, Boschi E (2012) A comparison of moment magnitude estimates for the European-Mediterranean and Italian regions. Geophys J Int 190:1733–1745. https://doi.org/10.1111/j.1365-246x.2012.05575.x

Ghielmi M, Minervini M, Nini C, Rogledi S, Rossi M, Vignolo S (2010) Sedimentary and tectonic evolution in the eastern Po-Plain and northern Adriatic Sea area from Messinian to Middle Pleistocene (Italy). Rendiconti Lincei 21(Suppl):131–166

Green RA, Cubrinovski M, Cox B, Wood C, Wotherspoon L, Bradley B, Maurer B (2014) Select Liquefaction case histories from the 2010–2011 canterbury earthquake sequence. Earthq Spectra 30(1):131–153

Guidoboni E, Ferrari G, Mariotti D, Comastri A, Tarabusi G, Sgattoni G, Valensise G (2018) CFTI5Med, Catalogo dei Forti Terremoti in Italia (461 a.C.1997) e nell'area Mediterranea (760 a.C.-1500). Istituto Nazionale di Geofisica e Vulcanologia (INGV). https://doi.org/10.6092/ingv.it-cfti5

Idriss IM, Boulanger RW (2008) Soil liquefaction during earthquakes. MNO-12, Earthquake Engineering Research Institute, Oakland, CA

Ishihara K (1985) Stability of natural deposits during earthquakes. In Vol 1 of Proc, 11th international conference on soil mechanics and foundation engineering, San Francisco 321–76

Iwasaki T, Tokida K, Tatsuoka F, Yasuda S, Sato H (1982) Microzonation for soil liquefaction potential using simplified methods. In: Vol 3 of Proc, 3rd Int Conf on Microzonation, 1319–1330

Juang CH, Fang SY, Khor EH (2006) First-order reliability method for probabilistic liquefaction triggering analysis using CPT. J Geotech Geoenviron Eng 132(3):337–350. https://doi.org/10.1061/(ASCE)1090-0241(2006)132:3(337)

Juang CH, Jiang T, Andrus RD (2002) Assessing probability based methods for liquefaction potential evaluation. J Geotech Geoenviron Eng 128(7):580–589. https://doi.org/10.1061/(ASCE)1090-0241(2002)128:7(580)

Kayen R, Moss RES, Thompson EM, Seed RB, Cetin KO, Der Kiureghian A, Tanaka Y, Tokimatsu K (2013) Shear-Wave velocity-based probabilistic and deterministic assessment of seismic soil liquefaction potential. J Geotech Geoenviron Eng 139(3):407–419. https://doi.org/10.1061/(ASCE)GT.1943-5606.0000743

Lai CG, Bozzoni F, Conca D, Famà A, Özcebe A G, Zuccolo E, Meisina C, Bonì R, Bordoni M, Cosentini RM, Martelli L, Poggi V, Viana da Fonseca A, Ferreira C, Rios S, Cordeiro D, Ramos C, Molina-Gómez F, Coelho C, Logar J, Maček M, Oblak A, Ozcep F, Bozbey I, Oztoprak S, Sargin S, Aysal N, Oser C, Kelesoglu MK (2020) Technical guidelines for the assessment of earthquake induced liquefaction hazard at urban scale. Bull Earthq Eng, 1–45

Lanzano G, Luzi L, Pacor F, Felicetta C, Puglia R, Sgobba S, D'Amico M (2019) A revised ground-motion prediction model for shallow crustal earthquakes in Italy. Bull Seismol Soc Am 109(2):525–540. https://doi.org/10.1785/0120180210

Locati M, Camassi R, Stucchi M (2011) DBMI11, la versione 2011 del Database Macrosismico Italiano, Milano, Bologna, Italy. http://doi.org/https://doi.org/10.6092/INGV.IT-DBMI11

Lugli S, Marchetti Dori S, Fontana D (2007) Alluvial sand composition as a tool to unravel the Late Quaternary sedimentation of the Modena Plain, northern Italy. In: Arribas J, Critelli S, Johnsson MJ (Eds.) Sedimentary Provenance and Petrogenesis: Perspectives from Petrography and Geochemistry, 420. Geol Soc Am Spec Pap, 57–72

Lugli S, Marchetti Dori S, Fontana D, Panini F (2004) Composition of sands in cores along the high-speed rail (TAV): preliminary indications on the sedimentary evolution of the Modena plain: Alpine and Mediterranean Quaternary, 17: 379–389

Marchetti S (2016) Incorporating the stress history parameter KD of DMT into the liquefaction correlations in clean uncemented sands. J Geotech Geoenviron Eng 142(2):04015072. https://doi.org/10.1061/(ASCE)GT.1943-5606.0001380

Marchetti S, Monaco P, Totani G, Calabrese M (2001) The flat dilatometer test (DMT) in Soil Investigations. A Report by the ISSMGE Committee TC16. In: Failmezger, RA, Anderson, JB (es), Proc Int Conf On Insitu Measurement of Soil Properties and Case Histories, Bali, 2001, official version reprinted in Flat Dilatometer Testing, Proc 2nd Int Conf On the Flat Dilatometer. Washington DC, April 2–5, 7–48

Martelli L (2021) Assessment of seismic bedrock in deep alluvial plains. Case studies from the Emilia-Romagna Plain. Geosciences 11(7):297. https://doi.org/10.3390/geosciences11070297

Martelli L, Bonini M, Calabrese L, Conti G, Ercolessi G, Molinari FC, Piccardi L, Pondrelli S, Sani F, Severi P (2017) Note illustrative della carta sismo tettonica della Regione Emilia-Romagna ed aree limitrofe. Regione Emilia-Romagna, Servizio Geologico, p 93

Martelli L, Calabrese L, Ercolessi G, Severi P, Romani M, Tarabusi G, Pileggi D, Rosselli S, Minarelli L, Pergalani F, Compagnoni M, Vannucchi G, Madiai C, Facciorusso J, Fioravante V, Giretti D, Mucciarelli M, Priolo E, Laurenzano G, Bramerini F, Speranza E, Conte C, Di Salvo G, Giuffrè M, Zuppiroli M, Guidi F, Vona V, Manicardi A, Mengoli B, Ugoletti C, Ricci L (2013) Microzonazione Sismica Dell'area Epicentrale Del Terremoto Della Pianura Emiliana Del 2012 (Ord. 70/2012). Atti 32° Convegno Nazionale GNGTS, Trieste. ISBN: 978–88–902101–7–4

Maurer B, Green R, Quigley M, Bastin S (2015) Development of magnitude-bound relations for paleoliquefaction analyses: New Zealand case study. Eng Geol 197:253–266. https://doi.org/10.1016/j.enggeo.2015.08.023

Meisina C, Bonì R, Bordoni M, Lai C, Famà A, Bozzoni F, Cosentini RM, Castaldini D, Fontana D, Lugli S, Ghinoi A, Martelli L, Severi P, (2019) 3D Geological model reconstruction for liquefaction hazard assessment in the Po Plain. Proc 7th International Conference on Earthquake Geotechnical Engineering, (ICEGE 2019). CRC Press, 2019 p 3837–3844

Michetti AM, Giardina F, Livio F, Mueller K, Serva L, Sileo G, Vittori E, Devoti R, Riguzz F, Carcano C, Rogledi S, Bonadeo L, Brunamonte F, Fioraso G (2012) Active compressional tectonics, Quaternary capable faults, and the seismic landscape of the Po Plain (northern Italy). Ann Geophys 55:969–1001. https://doi.org/10.4401/ag-5462

Michelini A, Faenza L, Lanzano G, Lauciani V, Jozinović D, Puglia R, Luzi L (2020) The new ShakeMap in Italy: progress and advances in the last 10 yr. Seismol Res Lett 91(1):317–333. https://doi.org/10.1785/0220190130

Minarelli L, Amoroso S, Tarabusi G, Stefani M, Pulelli G (2016) Down-hole geophysical characterization of middle-upper Quaternary sequences in the Apennine Foredeep, Mirabello, Italy. Ann Geophys 59(5):S0543. https://doi.org/10.4401/ag-7114, http://www.annalsofgeophysics.eu/index.php/annals/article/view/7114/6625

Moss RES (2003) CPT-based probabilistic assessment of seismic soil liquefaction initiation. PhD dissertation, Univ of California, Berkeley, CA

Moss RES, Seed RB, Kayen RE, Stewart JP, Kiureghian AD, Cetin KO (2006) CPT-based probabilistic and deterministic assessment of in situ seismic soil liquefaction potential. J Geotech Geoenviron Eng 132(8):1032–1051. https://doi.org/10.1061/(ASCE)1090-0241(2006)132:8(1032)

Paolucci R, Mazzieri I, Smerzini C (2015) Anatomy of strong ground motion: near-source records and three-dimensional physics-based numerical simulations of the Mw 6.0 2012 May 29 Po Plain earthquake, Italy. Geophys J in 203(3):2001–2020. https://doi.org/10.1093/gji/ggv405

Pezzo G, De Gori P, Lucente FP, Chiarabba C (2018) Pore pressure pulse drove the 2012 Emilia (Italy) series of earthquakes. Geophys Rese Lett 45:682–690. https://doi.org/10.1002/2017GL076110

Pizzi A, Scisciani V (2012) The May 2012 Emilia (Italy) earthquakes: preliminary interpretations on the seismogenic source and the origin of the coseismic ground effects. Ann Geophys 55(4):751–757

Pondrelli S (2002) European-Mediterranean Regional Centroid-Moment Tensors Catalog (RCMT). Istituto Nazionale di Geofisica e Vulcanologia (INGV). https://doi.org/10.13127/rcmt/euromed

Pondrelli S, Salimbeni S, Perfetti P, Danecek P (2012) Quick regional centroid moment tensor solutions for the Emilia 2012 (northern Italy) seismic sequence. Ann Geophys 55(4):615–621. https://doi.org/10.4401/ag-6146

Regione Emilia-Romagna (2012) Carta degli effetti di liquefazione osservati dopo i terremoti del 20 e 29 Maggio 2012. http://geo.regione.emilia-romagna.it/gstatico/documenti/liq2012/MAPPA_LIQUEFAZIONI_01.pdf

Regione Emilia-Romagna (2013) Sisma 2012 – Studi sismici, Ordinanza n 70 del 13/11/2012 e cartografia di riferimento (in Italian). http://ambiente.regione.emilia-romagna.it/geologia/temi/sismica/speciale-terremoto/sisma-2012-ordinanza-70-13-11-2012-cartografia

Robertson PK (2004) Evaluating Soil Liquefaction and Post-earthquake deformations using the CPT. Proc of 2nd Int Conf on Geotechnical and Geophysical Site Characterization – ISC'2, Porto 233–249

Robertson PK, Cabal KL (2015) Guide to Cone Penetration Testing for Geotechnical Engineering. Gregg drilling 6th edition July 2015

Robertson PK, Wride CE (1998) Evaluating cyclic liquefaction potential using the cone penetration test. Can Geotech J 35(3):442–459

Rollins KM, Amoroso S, Andersen P, Tonni L, Wissmann KJ (2021) Liquefaction mitigation of silty sands using rammed aggregate piers based on blast-induced liquefaction testing. J Geotech Geoenviron Eng. https://doi.org/10.1061/(ASCE)GT.1943-5606.0002563

Seed HB, Idriss IM (1971) Simplified procedure for evaluating soil liquefaction potential. J Soil Mech Found Div 97(9):1249–1273

Seed HB, Tokimatsu K, Harder LF, Chung RM (1985) The influence of SPT procedures in soil liquefaction resistance evaluations. J Geotech Eng 111(12):1425–1445. https://doi.org/10.1061/(ASCE)0733-9410(1985)111:12(1425)

Sinatra L, Foti S (2015) The role of aftershocks in the liquefaction phenomena caused by the Emilia 2012 seismic sequence. Soil Dyn Earthq Eng 75:234–245. https://doi.org/10.1016/j.soildyn.2015.03.024

Stefani S, Minarelli L, Fontana A, Hajdas I (2018) Regional deformation of late Quaternary fluvial sediments in the Apennines foreland basin (Emilia, Italy). Int J Earth Sci 107(7):2433–2447. https://doi.org/10.1007/s00531-018-1606-x

Stewart JP, Kramer SL, Kwak DY, Greenfield MW, Kayen RE, Tokimatsu K, Bray JD, Beyzaei CZ, Cubrinovski M, Sekiguchi T, Nakai S, Bozorgnia Y (2016) PEER-NGL project: open source global database and model development for the next-generation of liquefaction assessment procedures. Soil Dyn Earth Eng 91:317–328

Suzuki Y, Sanematsu T, Tokimatsu K (1998) Correlation between SPT and seismic CPT. In: Proc, Conf on Geotechnical Site Characterization, 1375–1380

Suzuki Y, Tokimatsu K, Moss RES, Seed RB, Kayen RE (2003) CPT-based liquefaction field case histories from the 1995 Hyogoken-Nambu (Kobe) Earthquake, Japan. Geotechnical Engineering Research Report No UCB/GE-2003/03

Tonni L, Gottardi G, Amoroso S, Bardotti R, Bonzi L, Chiaradonna A, d'Onofrio A, Fioravante V, Ghinelli A, Giretti D, Lanzo G, Madiai C, Marchi M, Martelli L, Monaco P, Porcino D, Razzano R, Rosselli S, Severi P, Silvestri F, Simeoni L, Vannucchi G, Aversa S (2015) Interpreting the deformation phenomena triggered by the 2012 Emilia seismic sequence on the Canale Diversivo di Burana banks. Riv Ital di Geotec, Anno XLIX, 2: 28–38. http://www.associazionegeotecnica.it/sites/default/files/rig/2_2015_028ton.pdf

Toscani G, Burrato P, Di Bucci D, Seno S, Valensise G (2009) Plio-Quaternary tectonic evolution of the northern Apennines thrustfronts (Bologna-Ferrara section, Italy): seismotectonic implications. Ital J Geosci 128:605–613. https://doi.org/10.3301/IJG.2009.128.2.605

Towhata I, Yasuda S, Yoshida K, Motohashi A, Sato S, Arai M (2016) Qualification of residential land from the viewpoint of liquefaction vulnerability. Soil Dyn Earthq Eng 91:260–271

Tsuchida H, Hayashi S (1971) Estimation of liquefaction potential of sandy soils. In: Proceedings of the 3rd Joint Meeting, US–Japan Panel on Wind and Seismic Effects, May 1971 UJNR, Tokyo, 91–109

van Ballegooy S, Malan P, Lacrosse V, Jacka ME, Cubrinovski M, Bray JD, O'Rourke TD, Crawford SA, Cowan H (2014) Assessment of liquefaction-induced land damage for residential Christchurch. Earthq Spectra 30(1):31–55

Wood CM, Cox BR, Green AG, Wotherspoon LM, Bradley BA, Cubrinovski M (2017) Vs-based evaluation of select liquefaction Case histories from the 2010–2011 Canterbury earthquake sequence. J Geotech Geoenviron Eng 143(9):04017066. https://doi.org/10.1061/(ASCE)GT.1943-5606.0001754

Zhang G, Robertson PK, Brachman RWI (2002) Estimating liquefaction induced ground settlements from CPT for level ground. Can Geotech J 39(5):1168–1180

Zimmaro P, Brandenberg SJ, Stewart JP, Kwak DY, Franke KW, Moss RES, Cetin KO, Can G, Ilgac M, Stamatakos J, Juckett M, Mukherjee J, Murphy Z, Ybarra S, Weaver T, Bozorgnia Y, Kramer SL (2019) Next-generation liquefaction database. next-generation liquefaction consortium. https://doi.org/10.21222/c2j040

Zuffa G (1985) Optical analyses of arenites: influence of methodology on compositional results. In: Zuffa G (Ed.) Provenance of Arenites: Dordrecht, Netherlands, D Reidel, NATO Advanced Study Institute, 148: 165–189